Field Measurements of Bottom Stress Due to Wave Action and Tidal Velocities in Tampa Bay to Support Seagrass Restoration and Shoreline Protection

A Study Funded by the Hillsborough County Environmental Protection Commission's Pollution Recovery Fund

Funding Granted to the Tampa Bay Estuary Program, Coastal Resources Group, Inc., and Marine Science Associates, Inc.

January 19, 2009

Sherryl Gilbert, M.S.
Marine Science Associates, Inc.
St. Petersburg, Florida

Bradley D. Robbins, Ph.D.
Coastal Ecosystem Division
South Florida Water Management District
West Palm Beach, FL

Mark E. Luther, Ph.D.
Marine Science Associates, Inc.
St. Petersburg, Florida

Roy R. Lewis III, M.A., P.W.S
Coastal Resources Group, Inc.
Salt Springs, Florida

Executive Summary

A two phase study during 2006-2008 collected *in situ* data as a precursor to development of realistic and spatially explicit wave models with which to explore the influences of both natural and anthropogenically derived waves (e.g. boat wakes) on seagrass meadows in Tampa Bay. While this was the initial and primary goal, data collection and preliminary results steered the study elsewhere.

The objective of the first phase of this study was to collect *in situ* data at five locations with different longshore bar systems to look at whether wave energy reductions could be detected in those locations with bars. Phase two of the study focused more on *in situ* data collection to quantify the total bed stress due to both wave action and tidal velocities at two locations, one with a distinct longshore bar system, and one without.

At all locations in Tampa Bay (Little Cockroach Bay, Piney Point, MacDill South, MacDill East Coffeepot Bayou and The Kitchen) it was concluded that wave energies inshore of the bar, on the bar, and offshore of the bar were not statistically different from one another. Simply looking at wave energies to determine overall energy regimes in these different regions was not enough to explain seagrass distribution in these regions. Explaining this may indicate that instrument position with relation to the links of a modified bar chain may play an important role in wave attenuation. This does not mean that wave energy is not a critical factor in seagrass distribution, but may reflect limited sampling over time and/or multiple parameters acting together, such as wave energy and tidal scour. More long term sampling and sampling both before and after future longshore bar construction projects will hopefully clarify these issues. Based upon data collected during this study, we suspect that tidal scour may be a largely undocumented factor that contributes along with wave energy to the stability, loss and recovery of seagrass beds in Tampa Bay.

Introduction

Seagrasses, found worldwide in the shallow subtidal and intertidal regions along continental coasts (McRoy and Helfferich 1977) are of primary interest to ecosystem managers. Autecological studies on seagrasses have documented that seagrass distribution is strongly related to physiology and growth characteristics including water depth and salinity zonation. Superimposed upon physiologically based constraints, however, are a variety of factors, such as impacts via grazing (Lewis 1987) or competitive interactions (Williams 1990), that may contribute to overall spatial arrangement of seagrass. Additionally, bioturbation (Fonseca *et al*. 1994), hydrodynamics (tidal currents, waves ***i.e.,*** Fonseca 1996; Fonseca and Bell 1998), and the variation of sediment grain size distribution across a site may influence both the arrangement (Mukai *et al*. 1980) and physical attributes of the seagrass across of suite of spatial scales (Fonseca 1996 and refs within).

Waves have long been recognized as important structural modifiers on the open coast, but only recently have we begun to model their dynamics within estuaries, especially in terms of how they influence habitat/ecosystem function and restoration success. Within Tampa Bay, the historical presence of long shore submarine bars was thought to attenuate the impact of wave energy on associated seagrasses; the loss of these bars and the corresponding loss of seagrasses within the Bay are thought to be tightly linked (Lewis et al. 1985) albeit not fully understood (Fonseca et al. 2002). Specifically, long shore sandbars that once existed throughout much of Tampa Bay were historically associated with healthy inshore and offshore seagrass meadows, which may have played a significant role in the temporal stability of the sandbars (Lewis 2002, Robbins et al. 2002). Water quality deterioration in the Bay during the early 20th Century resulted in a significant reduction in seagrass areal extent (Lewis et al. 1985), which may have lead to the destabilization of the long shore bars and subsequently the further erosion of seagrass landscape homogeneity as evidenced by the increased patchy distribution of seagrass beds in historically continuous seagrass meadows (*sensu* Fonseca and Bell 1998, Fonseca et al. 1998, Fonseca et al. 2002).

The maintenance of Tampa Bay's deep shipping channel by dredging may also have contributed to seagrass and longshore bar loss by creating a hydraulic situation and chronic bed stress where neither the bars nor the seagrass can effectively recover. Periodic long period waves resulting from the displacement of water within the deep channel by the movement of large ships may also contribute to the lack of recovery. This effect has not yet been sufficiently studied to provide a quantitative assessment of its role, if any, in limiting seagrass distribution.

The objective of the first phase of this study was to collect *in situ* data that may be used to develop realistic and spatially explicit wave models with which to explore the influences of both natural and anthropogenically derived waves (e.g. boat wakes) on seagrass meadows. Phase two of the study focused more on *in situ* data collection to quantify the total bed stress due to both wave action and tidal velocities.

Methodology for Phase 1

Early in 2006, five primary wave energy measurement sites (South MacDill AFB, East MacDill AFB, the Kitchen, Little Cockroach Bay, and Piney Point) within Tampa Bay, Hillsborough County, Forida (Figure 1) were chosen and classified with regard to the presence or absence of historic and/or current bars. On each, an array of three instruments (RBR TWR-2050 Submersible Tide and Wave recorders), which are capable of measuring waves (anthropogenic and wind-generated) were deployed perpendicular to the nearest shore and across a submerged bar area or its analog. Each deployment covered a seven-day period at a burst sample rate of 4Hz with a burst length of 512 (4 samples s^{-1} over time intervals of 8:32) resulting in the collection of ~2.5 million data points per instrument per deployment per site.

Instruments were deployed within PVC housings that were buried to a depth of 25 cm allowing the recorders to operate at very low tide heights (< 10 cm water depth).

Housings were made of 6 cm diameter PVC pipes measuring 35 cm in length. Buried ends were sealed with a solid cap, which allowed the pipe to be driven into the benthos. After placement of the housing a RBR recorder was inserted and the housing's end was sealed with a slotted cap affixed with small cable ties. Scraps (225 cm^2) of nylon stocking material were attached over the slotted end cap to act as a filter inhibiting the passage of sediment into the housing.

At the time of deployment, neither the East MacDill nor the Kitchen sites housed a submerged bar, while only a remnant bar was present at the South MacDill site. At the remaining two sites, the existing bar consisted of a series of small "broken" bars rather than as a large, single bar, which was probably present historically. With the exception of East MacDill a Nortek Vector 3D current meter was also deployed. This instrument was deployed outside the bar area in ~2.5 m of water where it captured current direction and speed as well as the physical characteristics of waves.

Data Processing and Analysis

Initial data processing of the RBR data was done using proprietary RBR software that allowed a calculation of two derived units: 1) depth; and 2) wave height ($H_{1/3}$) to be made from the raw data (pressure and temperature). A cursory examination of these plots (Figure 2 – 16) suggests that significant wave height (H_{max}) although superficially similar may be impacted by the presence of a bar. For example, at MacDill South wave heights were significantly different ($p < 0.0001$) among the instrument locations (Figures 2 – 4) with the middle instrument located on the remnant bar having a greater mean maximum wave height (H_{max}) than either instrument in front of or behind the remnant bar (Figure 5). Comparatively, this pattern was also true for sites without a bar (i.e., MacDill East; Figures 6 – 8, and the Kitchen; Figures 10-12) with the mean H_{max} values being significantly different ($p < 0.0001$) among instrument locations (Figures 9 and 13). This may indicate the diminutive nature of the remnant bar, which remains at the MacDill South site.

Both final two sites (Little Cockroach Bay and Piney Point; Figure 1) can be characterized as having a bar structure. However, unlike the MacDill South bar that lies parallel to the shoreline these bars make up a "broken chain" with individual links lying at an angle to the shoreline. Furthermore, although these bars are smaller in length and width than the MacDill South remnant bar, they are more distinct and consequently may be more effective at attenuating waves. Examining the wave profile at the Little Cockroach Bay site (Figures 14 – 16) might lead to the conclusion that no difference exists among the instrument stations. However, there was a significant difference ($p < 0.0001$) found with the mean H_{max} value at the inner station being less than either the middle (shoal) or outer stations (Figure 17). Interestingly there was little difference in the mean H_{max} values between the middle and outer stations. The Piney Point wave profiles (Figures 18-20) do indicate a difference among stations with the middle station appearing to be much noisier and with smaller amplitude than the other stations. However, a statistical comparison (Figure 21) reveals that the inner and middle stations are not statistically different from one another while both differ statistically form the outer

station. Explaining this dichotomy between the two sites is problematic but may indicate that instrument position with relation to the links of the bar chain may play an important role in wave attenuation.

Following this analysis we searched for a boat wake structure in the raw data time series with the hope of quantifying the amount of energy that would be introduced into a particular region from a forcing function such as a boat wake from both large and small vessels.

Initially we attempted to isolate wave bursts that contained a boat wake signature from all other data. Our strategy was to extract the maximum, minimum, and mean pressure value from each data burst, under the hypothesis that the first wave created by boat wake would dominate the burst. We found this was not necessarily true.

Second, we attempted to identify boat wake signatures by first amplifying the highest energy value within a wake signature by computing the ratio of the maximum to mean pressure value, before applying a 12.5 second "boxcar" to each wave burst at each time step (0.25 seconds) and computing the variance. This strategy was promising initially, but proved ineffective for more than 90% of the wave bursts. Consequently, wave bursts depicting boat wakes could not be identified by this method.

Third, we attempted to isolate the lower amplitude variability in the wave burst data by first removing the tidal components from the time series using the Forman Tidal analysis program (Pawlowicz et al., 2002). We then high pass filtered the residuals using a convolution filter with a cutoff at ~ 4 hrs and a filter width of 6 hrs (Bloomfield, 1976). The width of our filter was driven by the relatively short temporal nature of our observations. This strategy too did not reveal signatures of boat waves from the background wave signatures.

The inability of the above methods to extract boat wave structure prompted a quantitative overview of the frequency/energy structure of the full pressure series because of both waves being so close in frequency space. Thus we applied a fast Fourier transform (FFT) to each wave burst in an effort to provide a clearer picture of the frequencies that are dominant in introducing wave energies to this region.

After applying filters to remove tidal frequencies, we found large amplitude variability in the 0.25 to 0.5 s^{-1} frequency band that was modulated throughout the one week record with periodicity of ~24 hrs (Figures 22-26). We have not identified the source of this variability but hypothesize that other diurnal factors such as the local wind field may have influenced our data.

Because the results of the FFT showed higher amplitudes from waves with periods between 2 and 4 s, a complex demodulation was performed on the data using a period of 2.5 s. This was accomplished by multiplying the filtered time series by:

$$e^{-i\omega t}$$

where $\omega=2\pi/T$ and T is the period of interest. This resulted in a time series where any variability in the series could be attributed solely to the 2.5 s wave (Figures 27-31). Having a dominant periodicity provides us with a basic descriptor of overall wave energy.

We are able to compare sites and locations by looking at the energy variability in the demodulated time series. These series reiterate what was found in looking at the raw wave heights. The MacDill South on-bar location (Figure 30) shows higher amplitude than the inshore location, indicating that the bar structure dissipates wave energy. As seen in the wave heights, this also occurs at the Kitchen site where there is no bar structure present (Figure 27). The energy environment at the MacDill East site (Figure 29) and the two broken bar sites (Figure 28 and Figure 31), shows typical results with heights decreasing as we move onshore.

Conclusions for Phase 1 and Next Steps for Phase 2

Our initial analyses suggest that boat wakes may not the dominant feature in Tampa Bay, a predominantly wind-driven estuary. However, locally in Hillsborough Bay, cruise ships, cargo ships, and tugs do periodically create abnormally high waves (e.g. rogue waves) that may impact seagrasses, increase shoreline erosion, and are known to impact nesting seabirds on the exposed potions of the 2D and 3D dredged material disposal islands. Our analyses from this phase of the project show that energies from sources other than boat wake dominate the water level time series. Additional studies using visual observations and recordings of ship passages concurrent with in situ data may help to quantify ship wake energy and its impact on seagrass beds.

At all locations in Tampa Bay (Little Cockroach Bay, Piney Point, Mac Dill South, Kitchen, and Mac Dill East) it was concluded that wave energies inshore of the bar, on the bar, and offshore of the bar were not statistically different from one another. Simply looking at wind-driven wave energies to determine overall energy regimes in these different regions was not enough to explain seagrass distribution in these regions.

We suspect that tidal scour may be a factor. However, this was not a part of the initial phase of this project. We examine this possibility in the second phase of the project as discussed next.

Phase 2 Field Data Collection

In an effort to build upon the Phase I of the field study, two short-term deployments occurred in late April and early May of 2008. Wind-driven waves dominate the wave field in Tampa Bay, and in an effort to observe a high wave energy event, we chose a forecasted frontal passage for our first deployment (Figure 32) that coincided with the spring tide for that month (Figure 2). This deployment was carried out in Coffeepot Bayou from April 22nd to April 25th (Figure 3). The second deployment occurred off MacDill Air Force Base (Figure 4) from May 5th to May 12th to capture maximum tidal

velocities during another spring tide. Additionally, water level was approximately 25 cm above predicted due to strong southerly winds over this time period (Figure 5). A summary of sample locations and dates is shown in Table 1.

Table 1.

Location	In	Out	Profiles
Coffeepot Bayou Inshore 27° 46.999'N, 082° 37.068'W	4/22/08	4/25/08	159744
Coffeepot Bayou Offshore 27° 46.872'N, 082° 36.898'W	4/22/08	4/25/08	159744
MacDill AFB Inshore 27° 49.071'N, 082° 29.235'W	5/5/08	5/12/08	600064
MacDill AFB Offshore 27° 48.750'N, 082° 29.218'W	5/5/08	5/12/08	600064

At each location, a Sontek Pulse Coherent-Acoustic Doppler Profiler (PC-ADP) was deployed with a RBR pressure sensor. The ADP was upward looking and buried in the sediment for stability and to measure velocity as close to the seabed as possible. It measured the vertical velocity profile at 2 Hz for the first 17 minutes of every hour with a cell size of 5cm. The RBR pressure sensor measured temperature and pressure every 6 minutes, and collected a wave burst every 12 minutes at 4Hz for about 8.5 minutes.

Data Display

Data were uploaded upon instrument retrieval and analyzed with instrument-specific software. The raw time series of water level, wave heights, and temperature from the RBR from the Coffeepot deployment is shown in Figure 37. There are no temperature, water level, or wave data for the Coffeepot Bayou offshore location due to sensor malfunction. Eastward, northward, and vertical velocities for the same location are shown in figures 38 and 39. Only the first vertical cell is shown to view velocities closest to the sea bed. Figures 40 and 41 show data collected at the MacDill inshore and offshore sites, respectively while figures 42 and 43 show the eastward, northward, and vertical velocities from the Sontek ADP.

Discussion

Coffeepot Bayou

Both water level and wave heights are as expected at the inshore site. Water level ranges from 0.5 meters to 1.7 meters during this spring tide event. The high wind event began in the early morning hours of April 24th, and extended throughout the day. Wave heights at the inshore Coffeepot site began to ramp up on the morning of the 24th and peaked in the early afternoon. While wave action is observed at this site, heights are relatively low (2-4cm) and are not thought to contribute much energy to the bottom. Due to low voltage problems in the second sensor, we are unable to make comparisons between inshore and offshore wave data at Coffeepot Bayou.

While wave heights indicate the shallower inshore Coffeepot Bayou site as being low energy, the data from the ADP suggests otherwise. Both the eastward and northward components of velocity are larger at the inshore site than at the offshore site. Inshore, eastward velocities range from -137 cm/s to 139 cm/s with a mean of -0.55cm/s, northward velocities range from -145 cm/s to 133 cm/s with a mean of -0.35 cm/s.

Offshore, eastward velocities range from -102 cm/s to 90 cm/s with a small mean (0.27 cm/s) while the northward velocity is a bit larger with a range of -108 cm/s to 107 cm/s and a mean of 0.32 cm/s. The vertical velocities at both locations are more comparable with onshore ranges from -21cm/s to 20 cm/s an a mean of 0.45 cm/s and offshore ranges from -20 cm/s to 21.4 cm/s with a mean of only 0.15 cm/s. All three velocity components at the Coffeepot offshore site were significantly smaller than the more protected area at the inshore site.

Computing friction velocity provides a better way to quantify bed stress at the water-sediment interface. Friction velocity (U^*) is directly proportional to the bed stress. There are different methods available in the literature to compute friction velocity and here the Reynolds stress method is used (Soulsby, 1983). Voulgaris and Meyers (2004) evaluated the Reynolds stress method and the inertial dissipation method and found that the inertial dissipation method produces a shear velocity of about 15% larger than the Reynolds stress method. Therefore, we chose the Reynolds stress method as a conservative estimation of friction velocity and ultimately shear velocity. Figure 44 shows U^* for both Coffeepot Bayou sites in addition to the difference between the two. The inshore site experiences a much greater friction velocity than the offshore site. At this site, it is difficult to say if that friction velocity is predominantly due the wave energy or the tidal velocities because we do not have wave data at the offshore site, however, we do have both at the Mac Dill site.

One additional characteristic to note is that there is no preferred direction to the tidal velocities. Tidal ellipses were drawn from all sites (Figure 45) showing an equal distribution between the northward and eastward directions for both sites at both locations. This supports the decision to arbitrarily choose either direction (northward or eastward) for the computation of friction velocity and allows for using the raw velocity data without any rotation necessary.

MacDill

The maximum tidal range for both MacDill sites occurs on May 8th, decreasing towards the end of the deployment. Mean wave heights are higher at the offshore site as expected due to increased water depth, with a maximum of almost 60cm on May 12th and a 40cm wave height observed at the inshore site.

The velocity ranges are smaller at the inshore MacDill site than the Coffeepot inshore site, however the mean is larger. Eastward velocity ranges from -110 cm/s to 128 cm/s with a mean of 1.1 cm/s, northward velocities range from -118 cm/s to 113 cm/s with a

smaller mean at -0.18 cm/s, and vertical velocities range from -21 cm/s to 23 cm/s with a mean of 0.68 cm/s. Offshore eastward velocity ranges from -67 cm/s to 70 cm/s with a greater mean than the inshore component of 2.9 cm/s, northward components range from -68 cm/s to 60 cm/s with a smaller mean than the inshore site of 0.06 cm/s, and vertical velocities range from -11.6 cm/s to 13 cm/s with a smaller mean than the inshore site of 0.14 cm/s. Again, we must look at computed friction velocities to gain perspective on what is happening at the sediment water interface.

Figure 46 shows computed friction velocities at both MacDill sites. As at the Coffeepot site, inshore friction velocities are larger than the offshore friction velocities. Wave heights are larger at the offshore MacDill site than at the inshore site, indicating that this increase in friction velocity is due to the shear in the tidal velocities rather than from wave energy.

One additional variable we did not investigate was the sediment type and grain size at both the MacDill and Coffeepot sites. Qualitatively, the sediment was much finer at both MacDill sites making visibility during deployment and retrieval difficult, while the larger grain sediment at the Coffeepot site allowed for better visibility. During retrieval at MacDill, considerable erosion/bottom scour was observed (see Figure 51 a, b). However, no attempt was made to quantify particle size for this study.

It is worthwhile to note that Avery and Johansson (2006) reporting on the initial success of shoal grass transplants in Hillsborough Bay, noted that later failure could have been due to several causes including the passage of a 40-50 cm high sand ridge through the transplant site. Such large scale sand ridge formation and movement within shallow water areas of Tampa Bay has not been previously reported and may constitute an additional stressor to seagrasses and seagrass transplants due to similar inshore tidal velocities and the resulting frictional shear leading to meso-scale sediment movement.

Boat Wakes

An additional objective we chose to revisit in phase two of this study was the effect of boat wake energy at the sediment water interface. As we learned previously, extracting boat wake from pressure time series proves to be no simple endeavor. Boat wake structures vary depending on what kind of vessel creates the wake. In this study, the type of vessel that was responsible for the boat wake was not a priority, however, how the boat wake energy changed as it moved onshore from changing bathymetry due to submerged bar was. Each individual wave burst time series from the MacDill pressure series was examined for evidence of a boat wake. Figures 47 and 48 show two examples of a boat wake observed at the MacDill offshore site along with the observed corresponding eastward velocities and computed friction velocities. The falling water level and subsequent peaks are rather obvious as are the peaks in the velocities and the friction velocities. This was something that was not observed in the previous phase. We also wanted to investigate the possibility of wave attenuation due to the submerged bar as the wake moves from offshore to onshore. A signature of the same wake is present at the

MacDill inshore site; however, the orbital velocities may not reach the seabed since there is no peak in velocity or friction velocity as seen by Figures 49 and 50.

While Tampa Bay is predominantly a tidal and wind driven estuary, there exist other anthropogenic sources of disturbances that may have an impact on the distribution of seagrass beds and some of these impacts are difficult to quantify. Most of our results were contradictory to what we initially predicted. We observed larger tidal velocities in shallower regions and inshore of existing bars and smaller velocities at the deeper offshore sites. This may be due to an acceleration as the flow of water column moves from deeper water into shallower water. From the shape of the tidal ellipses, a similar volume of water is flowing through both deep and shallow locations but with very different depths; therefore, the shallower depth must have higher velocity to convey same volume. One other explanation for the enexpected results could be an artifact of having only one sensor at the inshore site. Water movement in shallow regions can follow subtle channels with increased velocities (Johansson, 2009). Wave action offshore and inshore of a submerged bar does not appear to be significantly different, indicating that these bars attenuate wave action very little, if at all. However, there may be an exception to this case, as was hypothesized in the initial phase of this project. Evidence at the MacDill site does support the idea that these submerged bars assist in the dampening of wave energy from boat wakes as they move onshore. The installation of additional or supplementary submerged bars may decrease bottom stress onshore and prevent further scouring. However, the submerged bars themselves may ultimately cause scouring by diverting wave energies or tidal flows around the structures (Palmer, 2009). Such an experimental installation of a longshore bars system at MacDill has been funded by the Pinellas County Environmental Fund and the U.S. Environmental Protection Agency and should be constructed during 2009.

Literature Cited

Avery, W., and R. Johansson. 2006. Experimental *Halodule wrightii* and *Syringodium filiforme* transplanting in Hillsborough Bay, Florida. Pages 91-101 in S.F. Treat and R.R. Lewis III
(Eds.), Seagrass Restoration: Success, Failure and the Cost of Both. Proceedings of the Conference. Mote Marine Laboratory, March, 2003. Lewis Environmental Services, Inc., Tampa, Florida. 175 p.

Bloomfield, R. 1976. Fourier Analysis of Time Series: An Introduction. John Wiley & Sons, New York, 258 pp

Fonseca, M.S. 1996. The role of seagrasses in nearshore sedimentary process. A review. Pages 261-286 in C. Roman and K. Nordstrom (Eds.) Estuarine Shores Hydrological, Geomorphological and Ecological Interactions. Blackwell, Boston, Massachusetts, USA.

Fonseca, M. S., and S. S. Bell. 1998. Influence of physical setting on seagrass landscapes near Beaufort, North Carolina, USA. Mar. Ecol. Prog. Ser. 171:109-121.

Fonseca, M.S., W.J. Kenworthy, F.X Courtney and M.O. Hall. 1994. Seagrass planting in the southeastern United States: methods for accelerating habitat development. Restor. Ecol. 2(3):198-212.

Fonseca, M.S., W.J. Kenworthy and G.W. Thayer. 1998. Guidelines for the conservation and restoration of seagrasses in the United States and adjacent waters. NOAA Coastal Ocean Program. Decision Analysis Series No. 12. NOAA, Beaufort, NC.

Fonseca, M.S., B. D. Robbins, P.E. Whitfield, L. Wood and P. Clinton. 2002. Evaluating the effect of offshore sandbars on seagrass recovery and restoration in Tampa Bay through ecological forecasting and hindcasting of exposure to waves. Tampa Bay Estuary Program, St. Petersburg, Florida. 21 p + appends.

R. Johansson. 2009. Personal communication.

Lewis, F.G. III. 1987. Crustacean epifaunal of seagrass and macroalgae in Apalachee Bay, Florida, USA. Mar. Biol. 94:212-229.

Lewis, R.R. 2002. The potential importance of the longshore bar system to the persistence and restoration of Tampa Bay seagrass meadows. Pages 177-183 in H.S. Greening (Ed.), Seagrass management: it's not just nutrients! Proceedings of a Symposium, August 22-24, 2000, St. Petersburg, Florida Tampa Bay Estuary Program, St. Petersburg, Florida.

Lewis, R. R., M.J. Durako, M.D. Moffler and R.C. Phillips. 1985. Seagrass meadows in Tampa Bay - A review. Pages 210-246 in S. F. Treat, J. L. Simon, R. R. Lewis III and R.

L Whitman, Jr. (eds.), Proceedings, Tampa Bay Area Scientific Information Symposium [May 1982]. Burgess Publishing Co., Minneapolis. 663 pp.

McRoy, C.P., C. Helfferich. 1977. Seagrass ecosystems. Marchel Dekker, Inc. New York.

Mukai, H., K. Aioi, Y. Ishida. 1980. Distribution and biomass of eelgrass (*Zostera marina*) and other seagrasses in Odawa Bay, Central Japan. Aquatic Botany, 8:337-342.

Palmer, M. A. 2009. Reforming Watershed Restoration: Science in Need of Application and Applications in Need of Science, Estuaries and Coasts, 32:1,1-17.

Pawlowicz, R. B. Beardsley, and S. Lentz. 2002. Classical tidal harmonic analysis including
error estimates in MATLAB using T_TIDE. Computers and Geosciences 28:929-937.

Robbins, B.D., M.S. Fonseca, P. Whitfield and P. Clinton. 2002. Use of a wave exposure technique for predicting distribution and ecological characteristics of seagrass ecosystems. Pages 171-176 in H.S. Greening (Ed.), Seagrass management: it's not just nutrients! Proceedings of a Symposium, August 22-24, 2000, St. Petersburg, Florida Tampa Bay Estuary Program, St. Petersburg, Florida.

Soulsby, R. L. 1983. The bottom boundary layer of shelf seas. In: Johns, B. (Ed.), Physical Oceanography of Coastal and Shelf Seas, vol. 35. Elsevier Oceanography Series, pp189-266.

Voulgaris, G., and S. T. Meyers. 2005. Temporal variability of hydrodynamics, concentration and sediment settling in a tidal creek. Continental Shelf Research, 24:1659-1683.

Williams, S.L. 1990. Experimental studies of Caribbean seagrass bed development. Ecol. Monogr. 60:440-469.

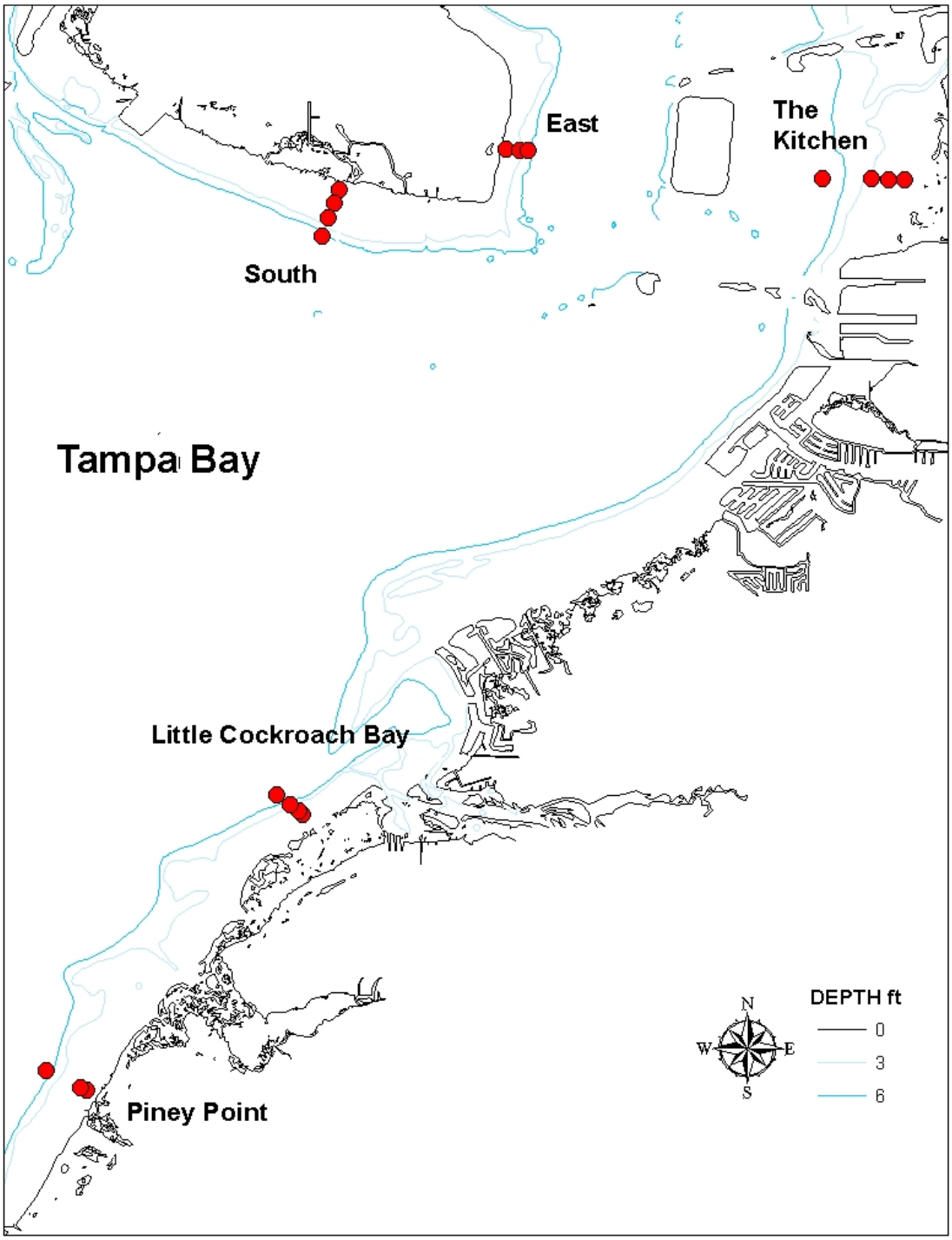

Figure 1: Specific site map illustrating the instrument array with relation to the shoreline and to bathymetric contours.

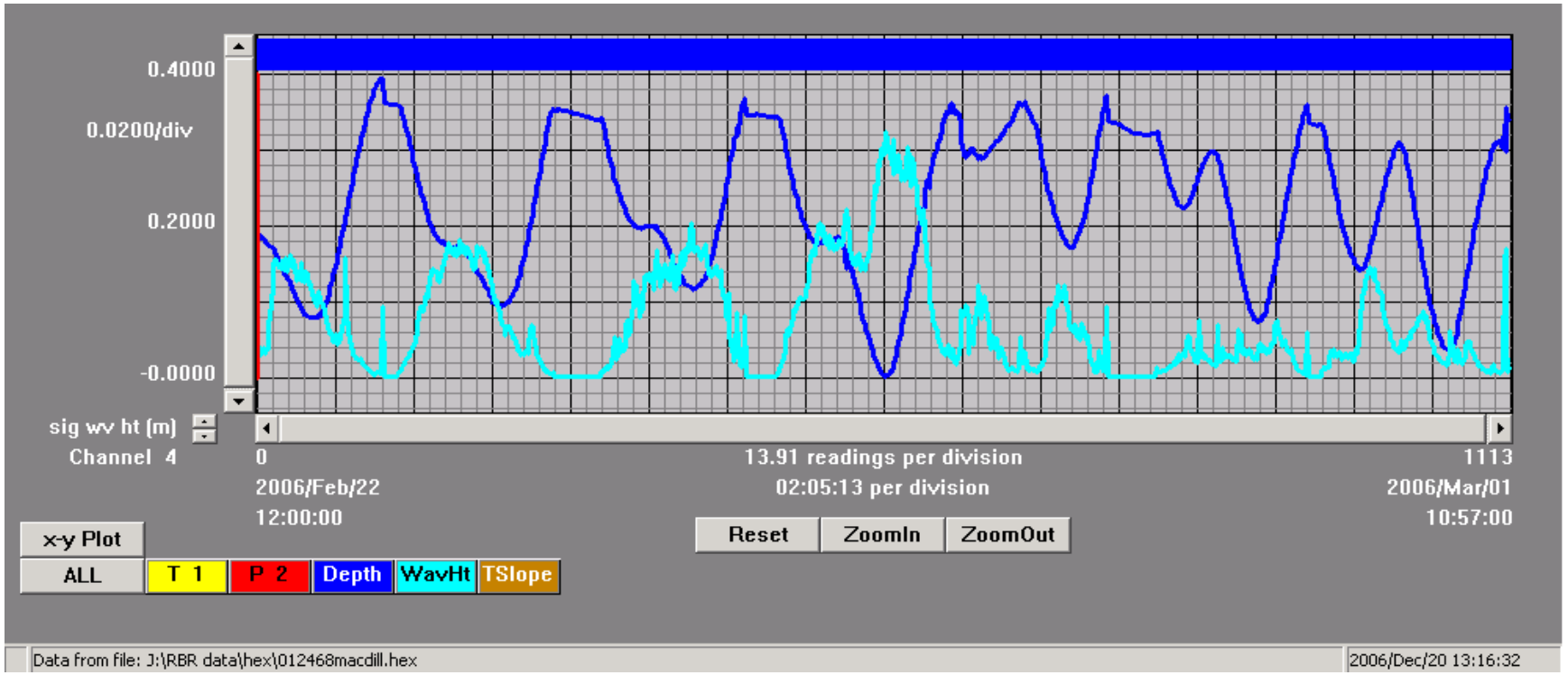

Figure 2: RBR data summary from MacDill AFB South. These data represent wave heights (H_{max}) and depth in front of the bar or its analog. Data were collected from March 8 – March 15, 2006.

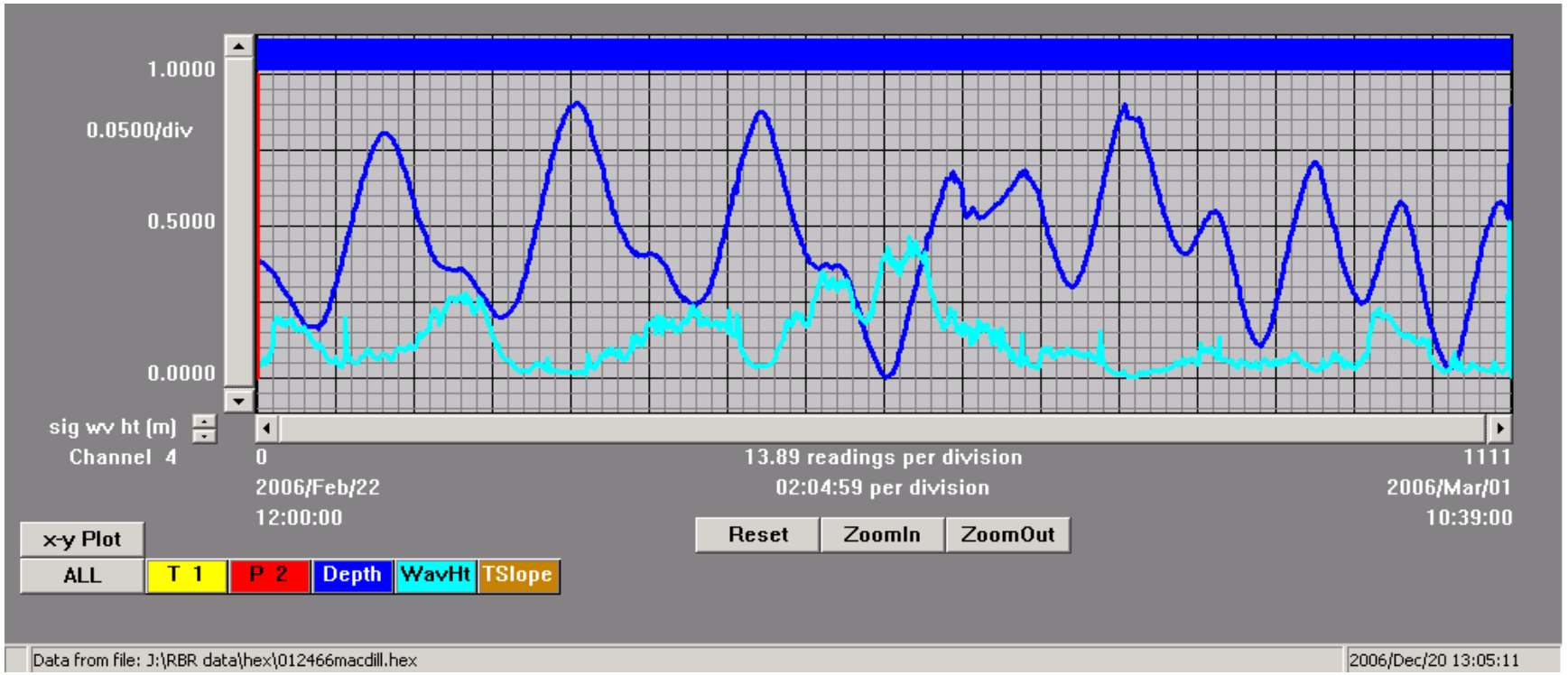

Figure 3: RBR data summary from MacDill AFB South. These data represent wave heights (H_{max}) and depth on the bar or its analog. Data were collected from February 22 – March 1, 2006.

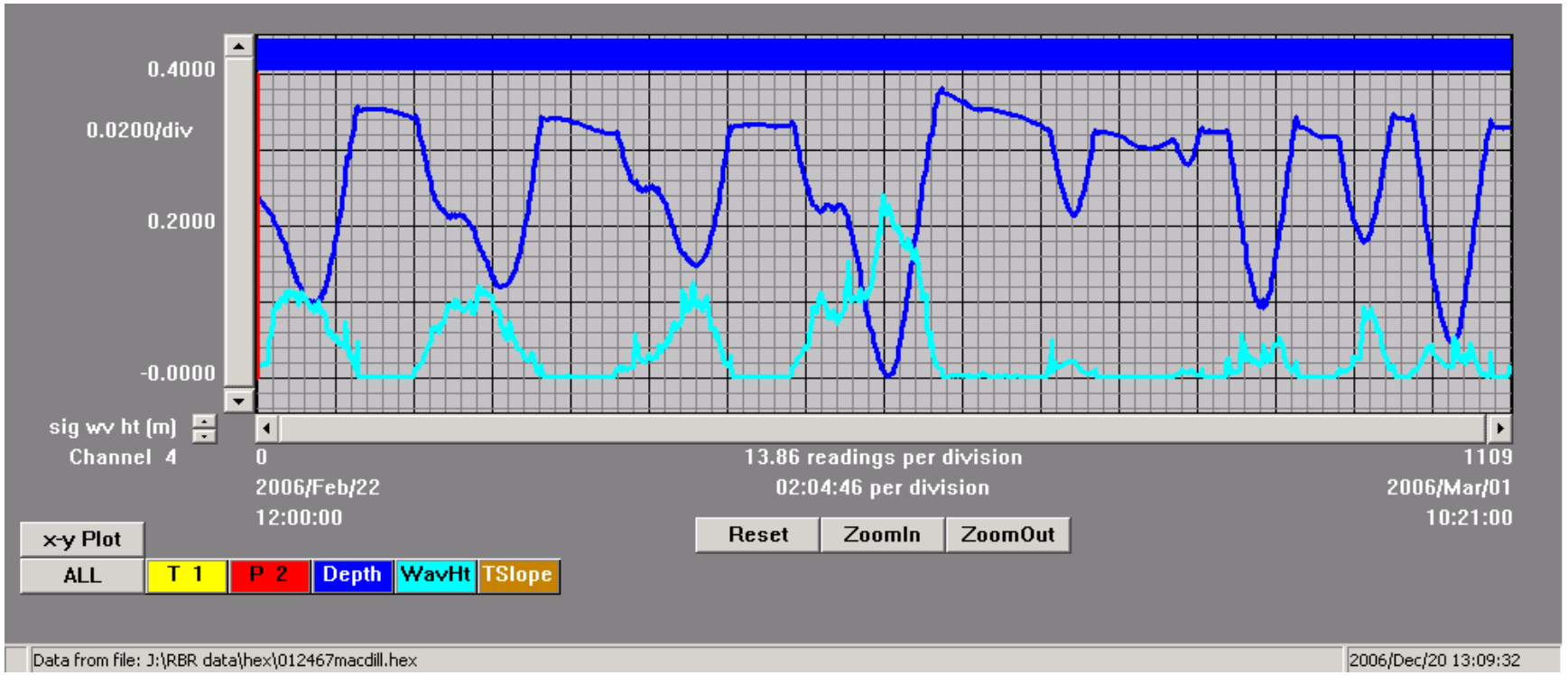

Figure 4: RBR data summary from MacDill AFB South. These data represent wave heights (H_{max}) and depth behind the bar or its analog. Data were collected from February 22 – March 1, 2006.

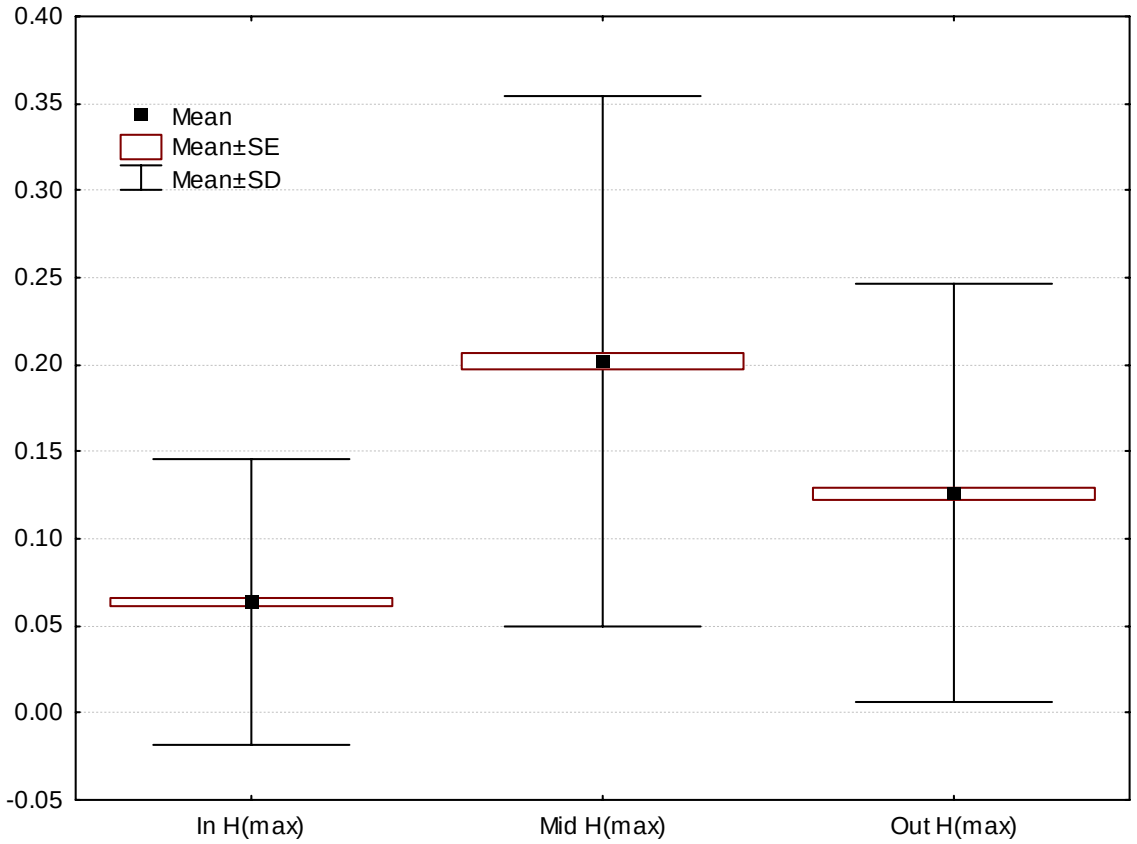

Figure 5: Box and Whisker plot depicting the relationship among instrument locations at the MacDill South site. Differences are significant at $p < 0.0001$.

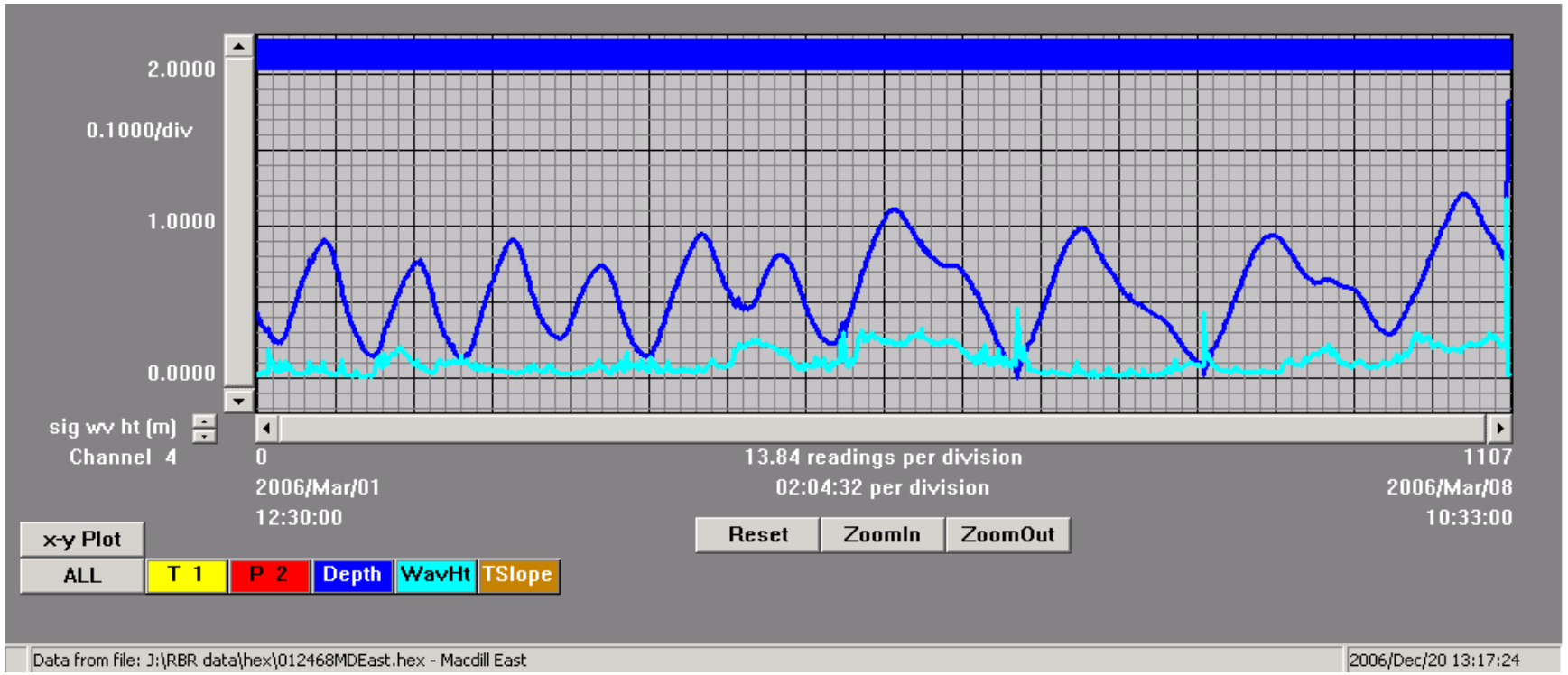

Figure 6: RBR data summary from MacDill AFB East. These data represent wave heights (H_{max}) and depth in front of the bar or its analog. Data were collected from February 22 – March 1, 2006.

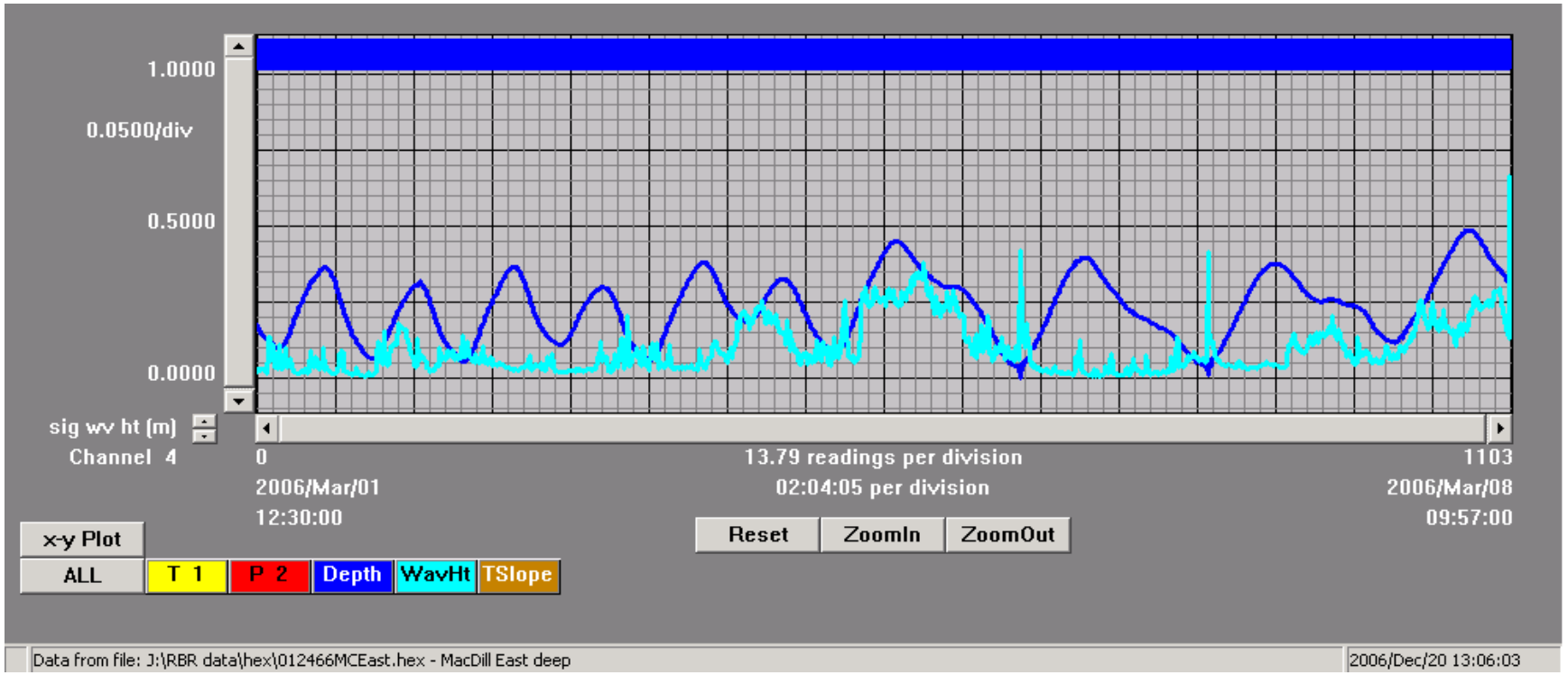

Figure 7: RBR data summary from MacDill AFB East. These data represent wave heights (H_{max}) and depth on the bar or its analog. Data were collected from March 1 – March 8, 2006.

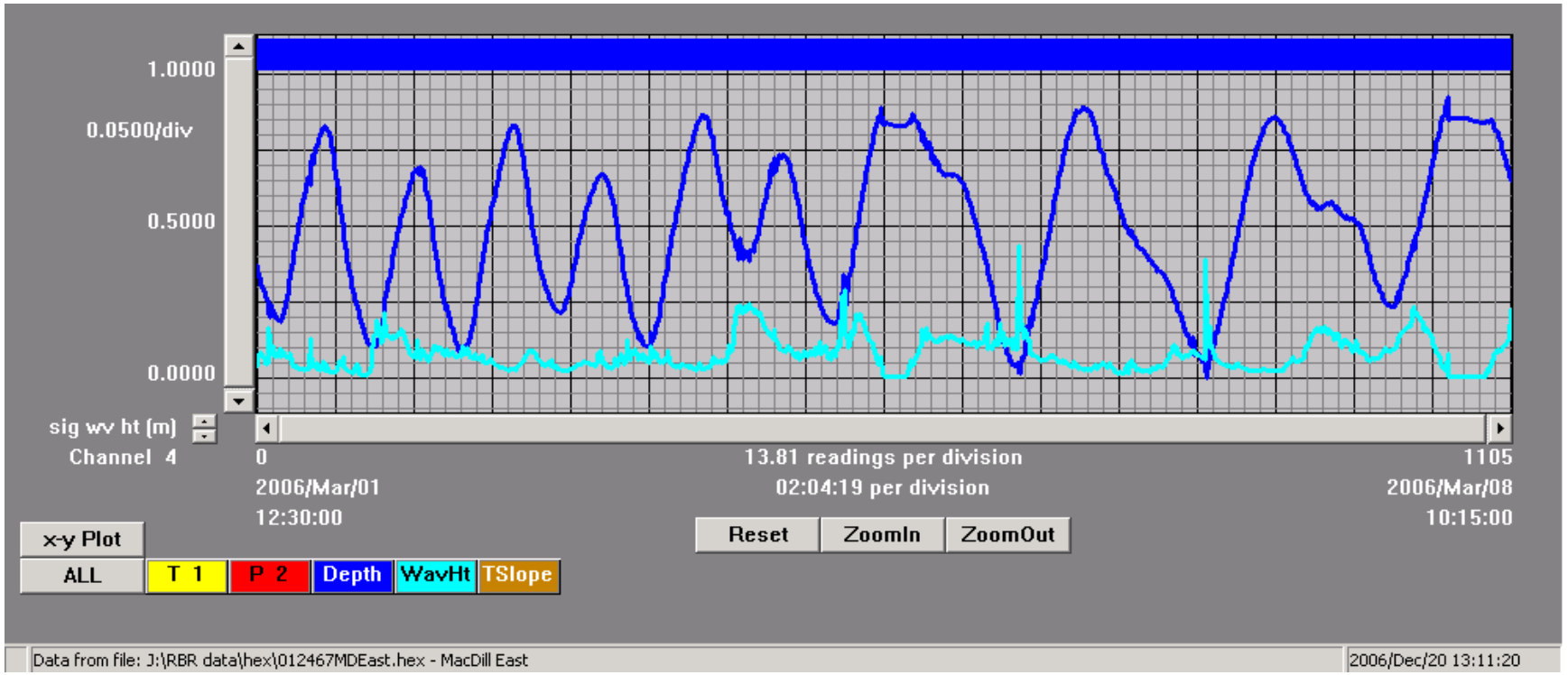

Figure 8: RBR data summary from MacDill AFB East. These data represent wave heights (H_{max}) and depth behind the bar or its analog. Data were collected from March 1 – March 8, 2006.

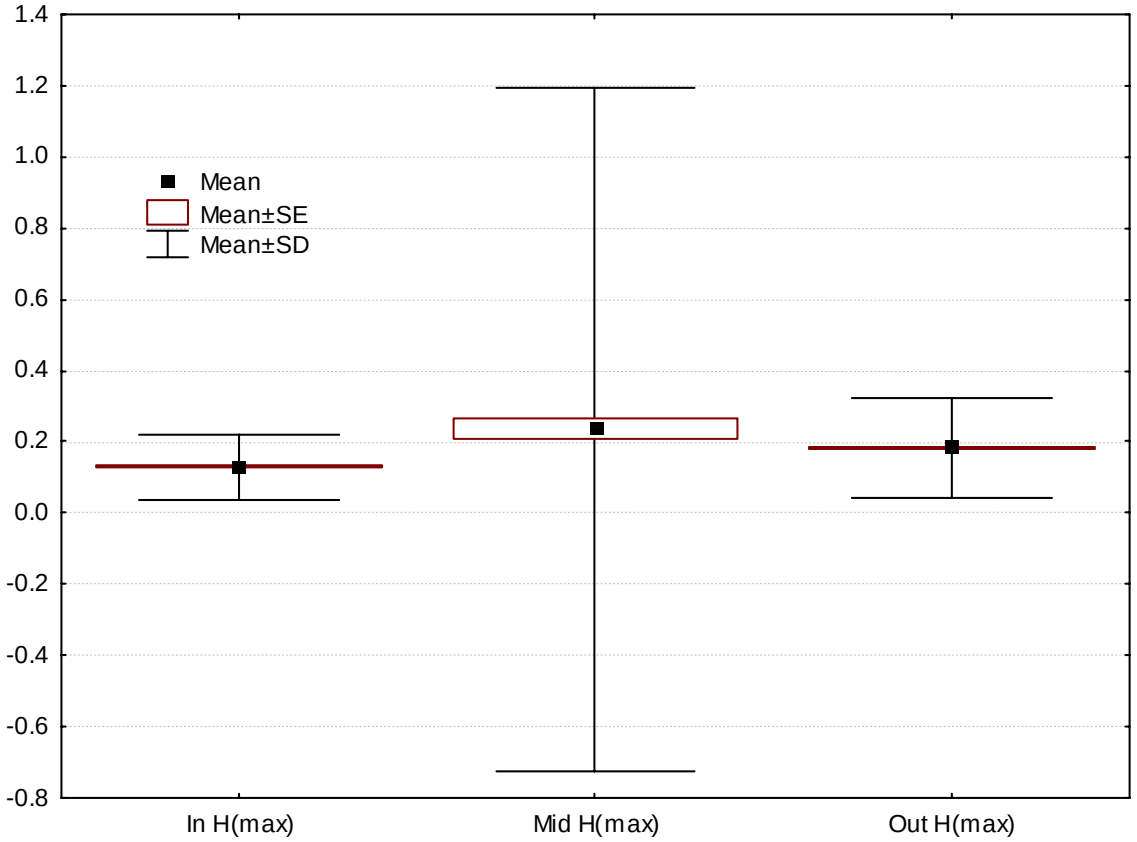

Figure 9: Box and Whisker plot depicting the relationship among instrument locations at the MacDill East site. Differences are significant at $p < 0.0001$.

Figure 10: RBR data summary from the Kitchen. These data represent wave heights (H_{max}) and depth in front of the bar or its analog. Data were collected from April 19 – April 26, 2006.

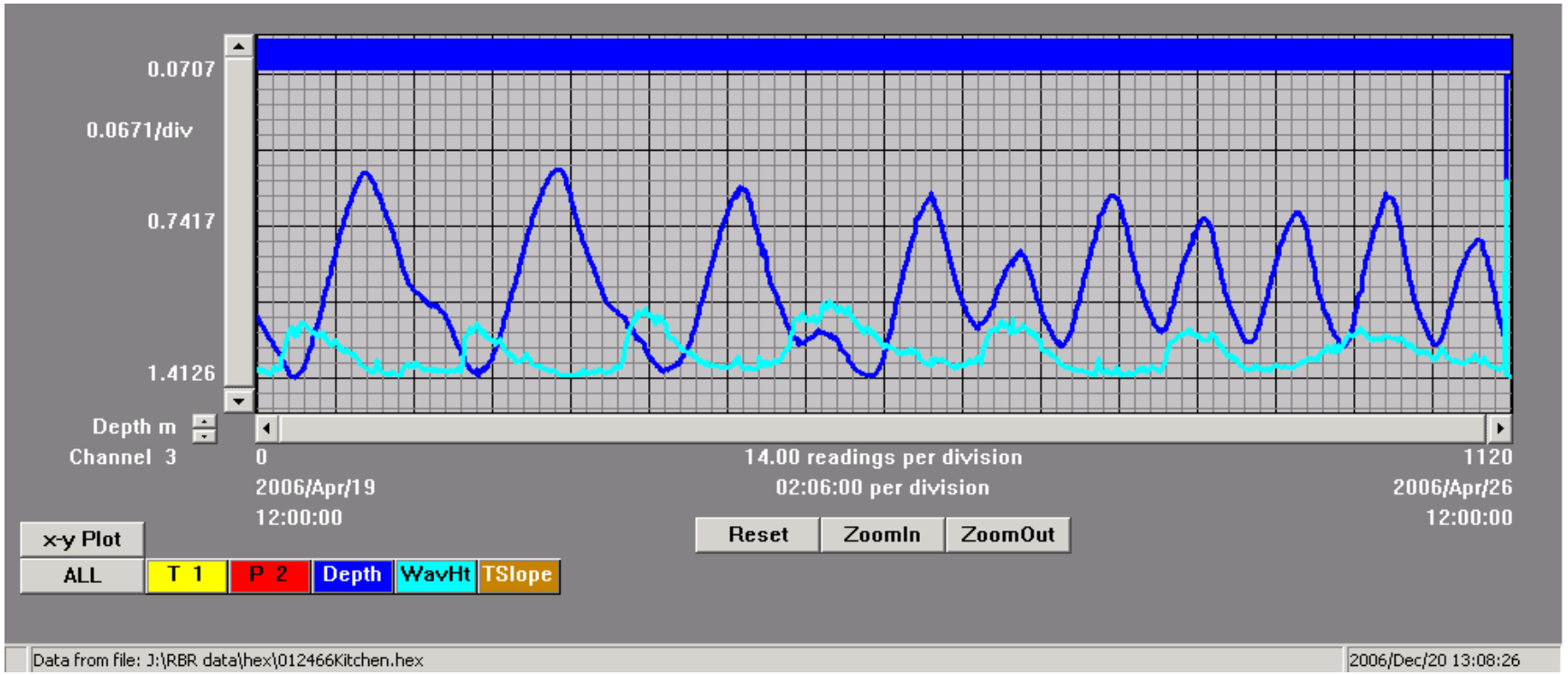

Figure 11: RBR data summary from the Kitchen. These data represent wave heights (H_{max}) and depth on the bar or its analog. Data were collected from April 19 – April 26, 2006.

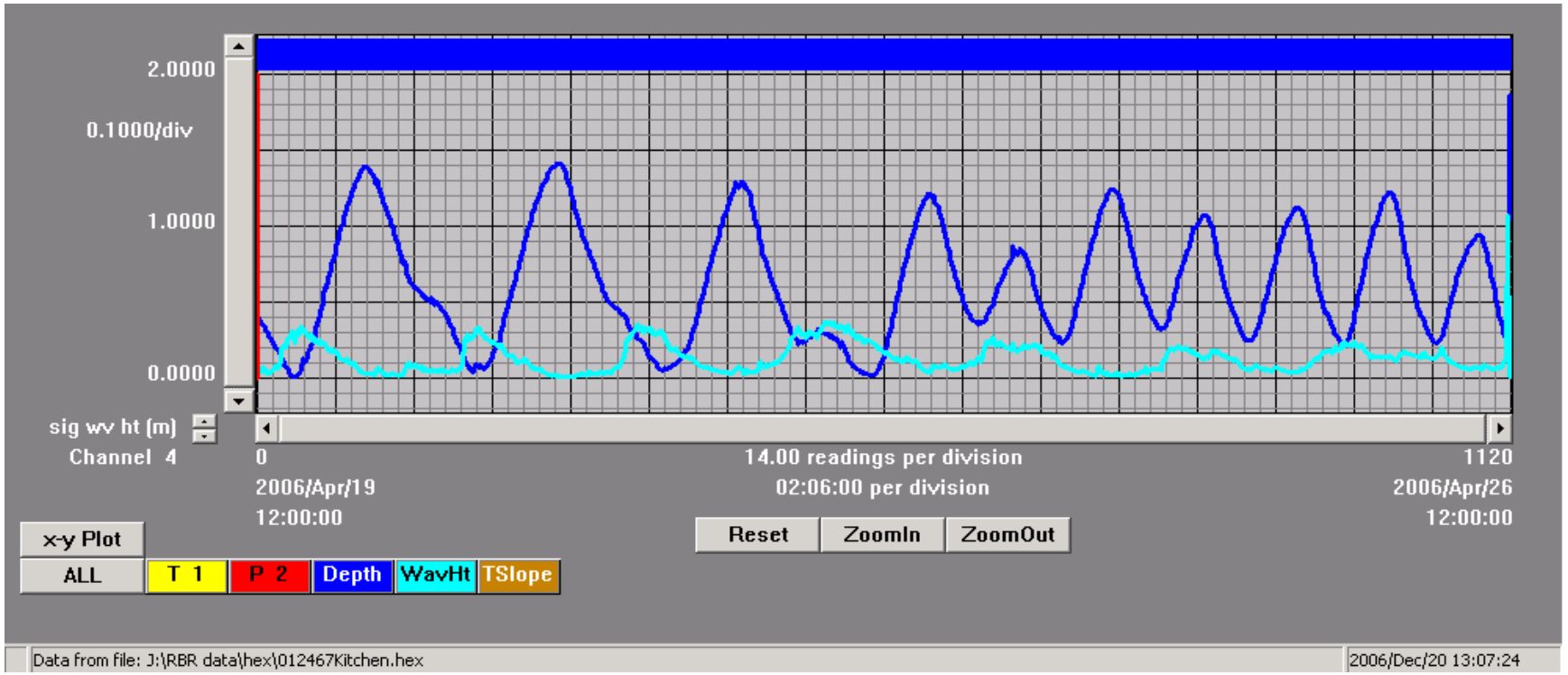

Figure 12: RBR data summary from the Kitchen. These data represent wave heights (H_{max}) and depth behind the bar or its analog. Data were collected from April 19 – April 26, 2006.

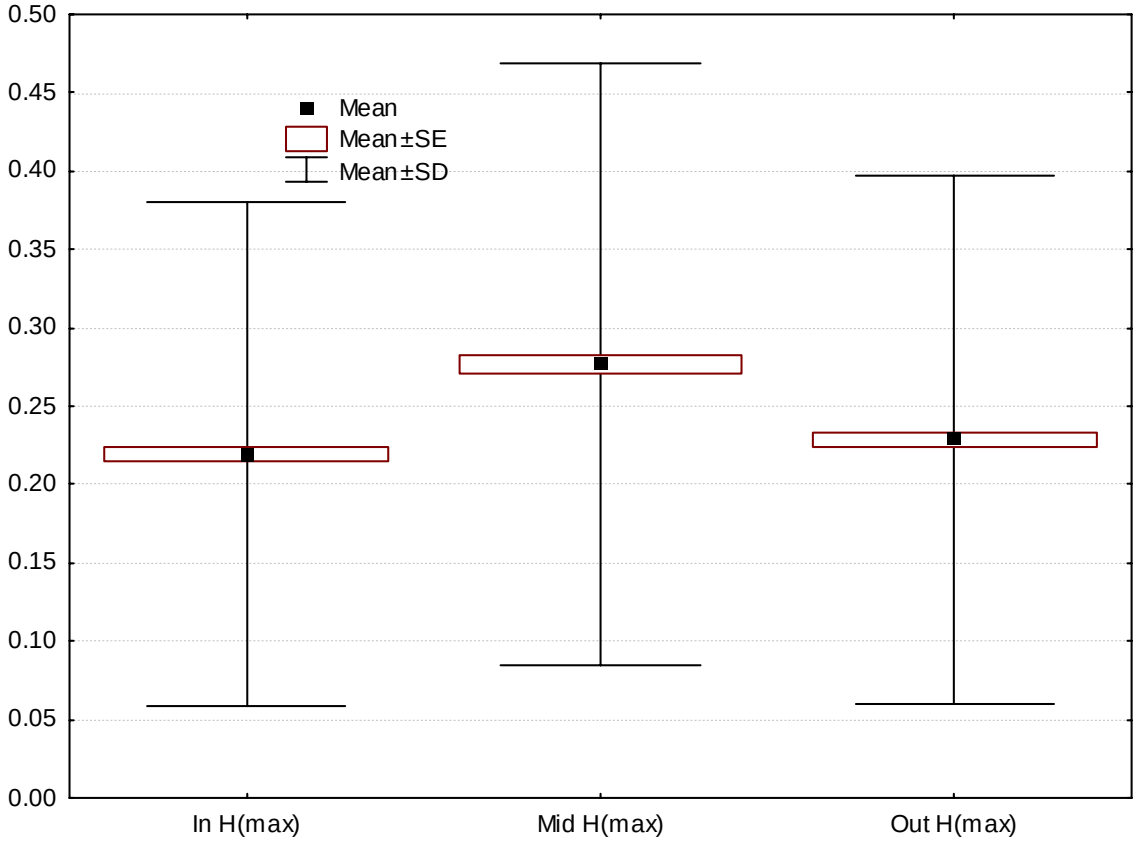

Figure 13: Box and Whisker plot depicting the relationship among instrument locations at the Kitchen site. Differences are significant at $p < 0.0001$.

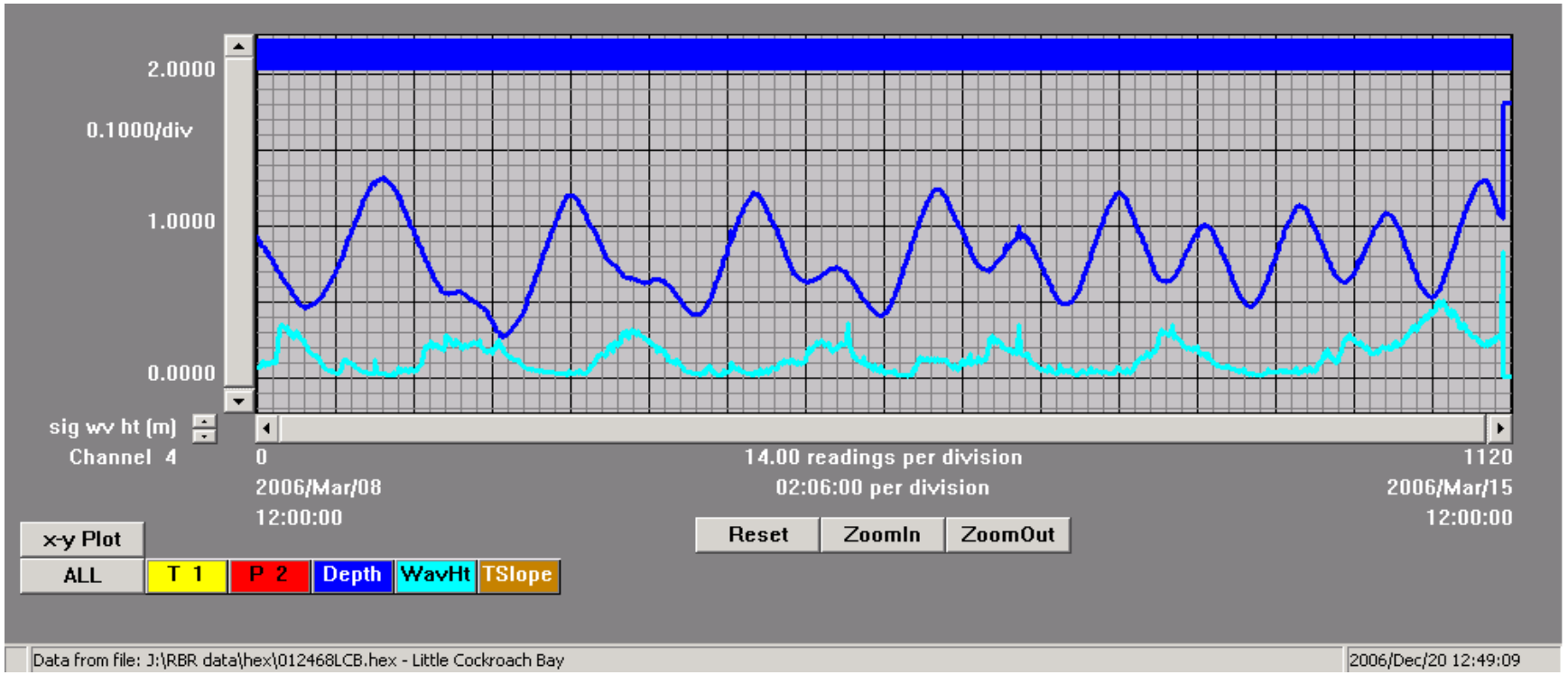

Figure 14: RBR data summary from Little Cockroach Bay. These data represent wave heights (H_{max}) and depth in front of the bar or its analog. Data were collected from March 8 – March 15, 2006.

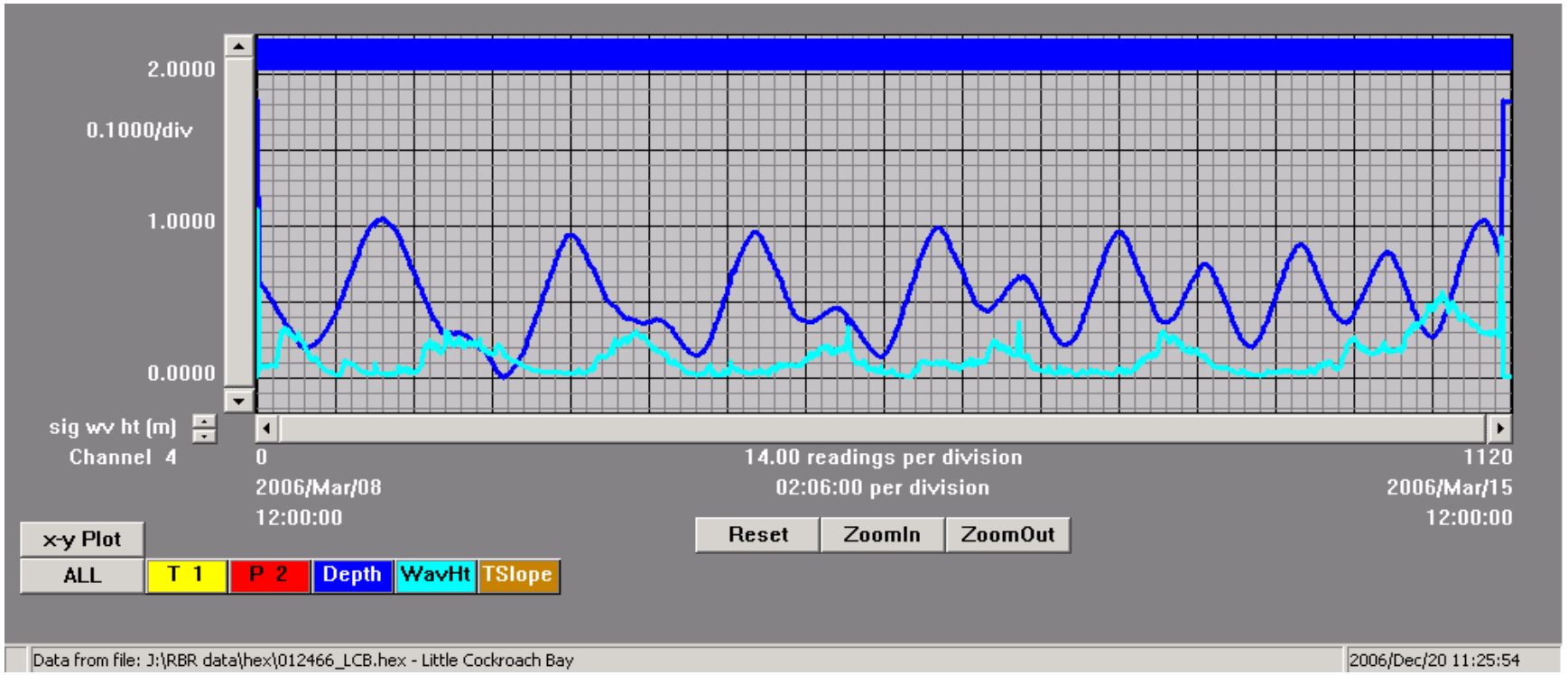

Figure 15: RBR data summary from Little Cockroach Bay. These data represent wave heights (H_{max}) and depth on the bar or its analog. Data were collected from March 8 – March 15, 2006.

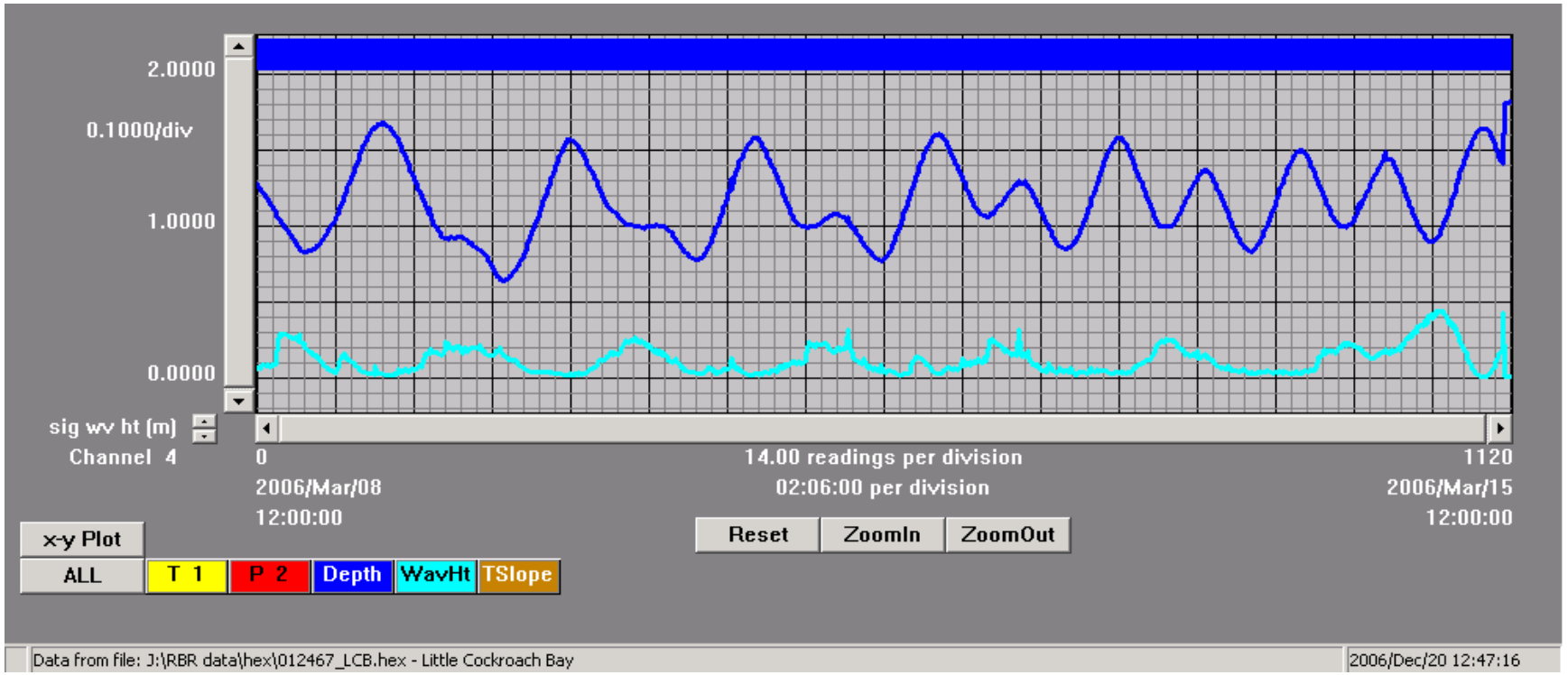

Figure 16: RBR data summary from Little Cockroach Bay. These data represent wave heights (H_{max}) and depth behind the bar or its analog. Data were collected from March 8 – March 15, 2006.

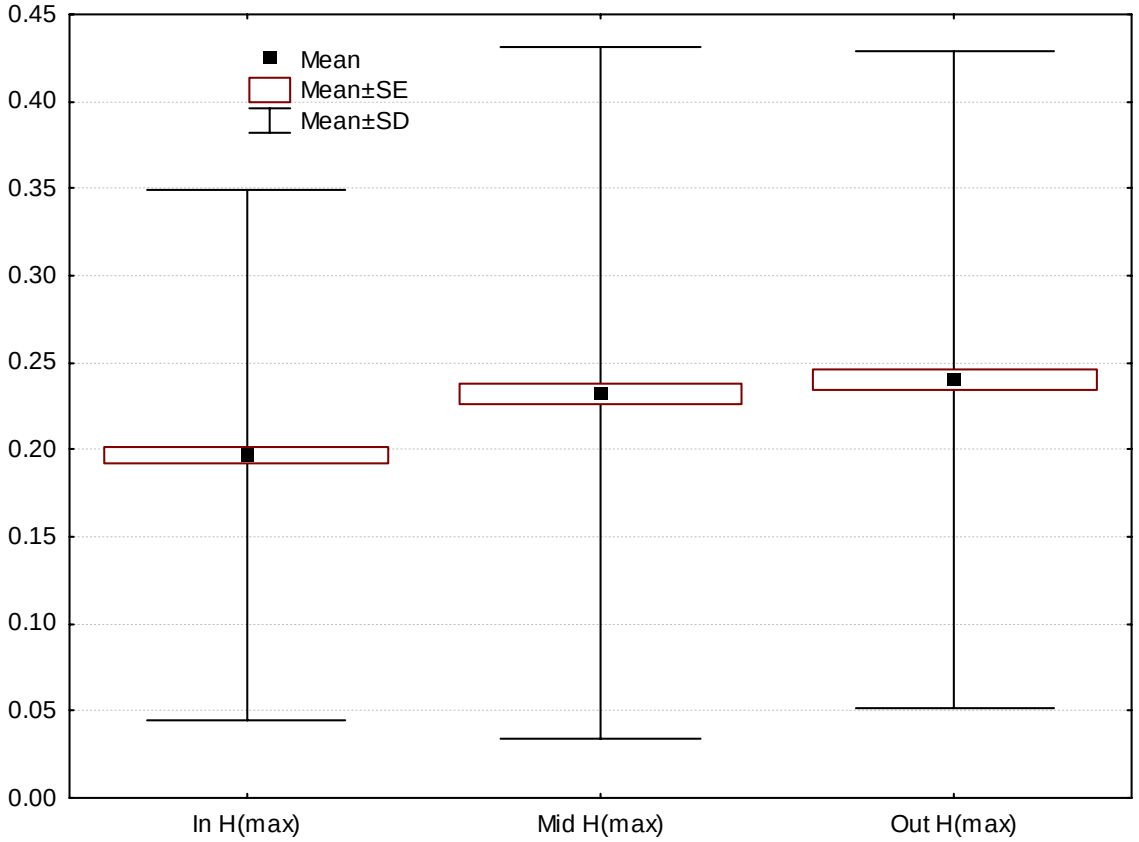

Figure 17: Box and Whisker plot depicting the relationship among instrument locations at the Little Cockroach Bay site. Differences are significant at $p < 0.0001$.

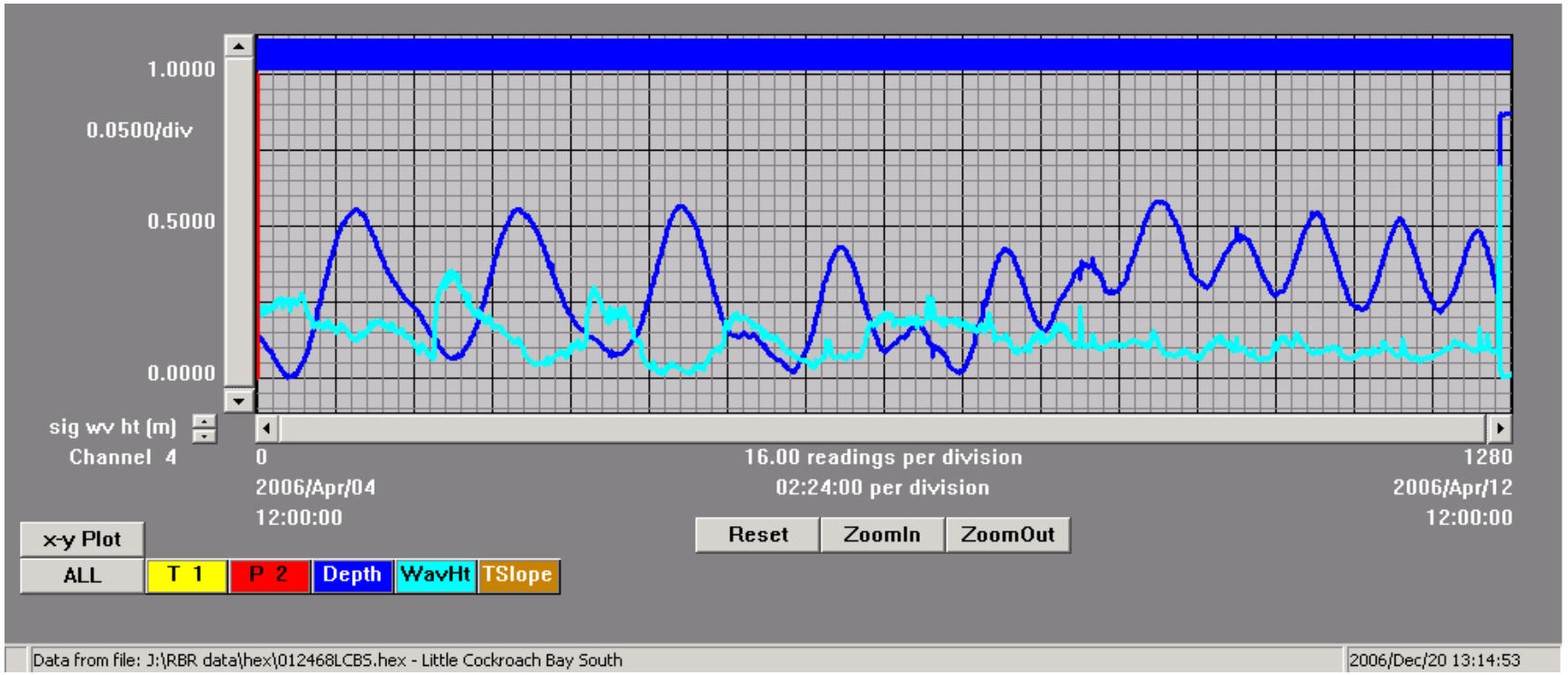

Figure 18: RBR data summary from Piney Point. These data represent wave heights (H_{max}) and depth in front of the bar or its analog. Data were collected from April 4 – April 12, 2006.

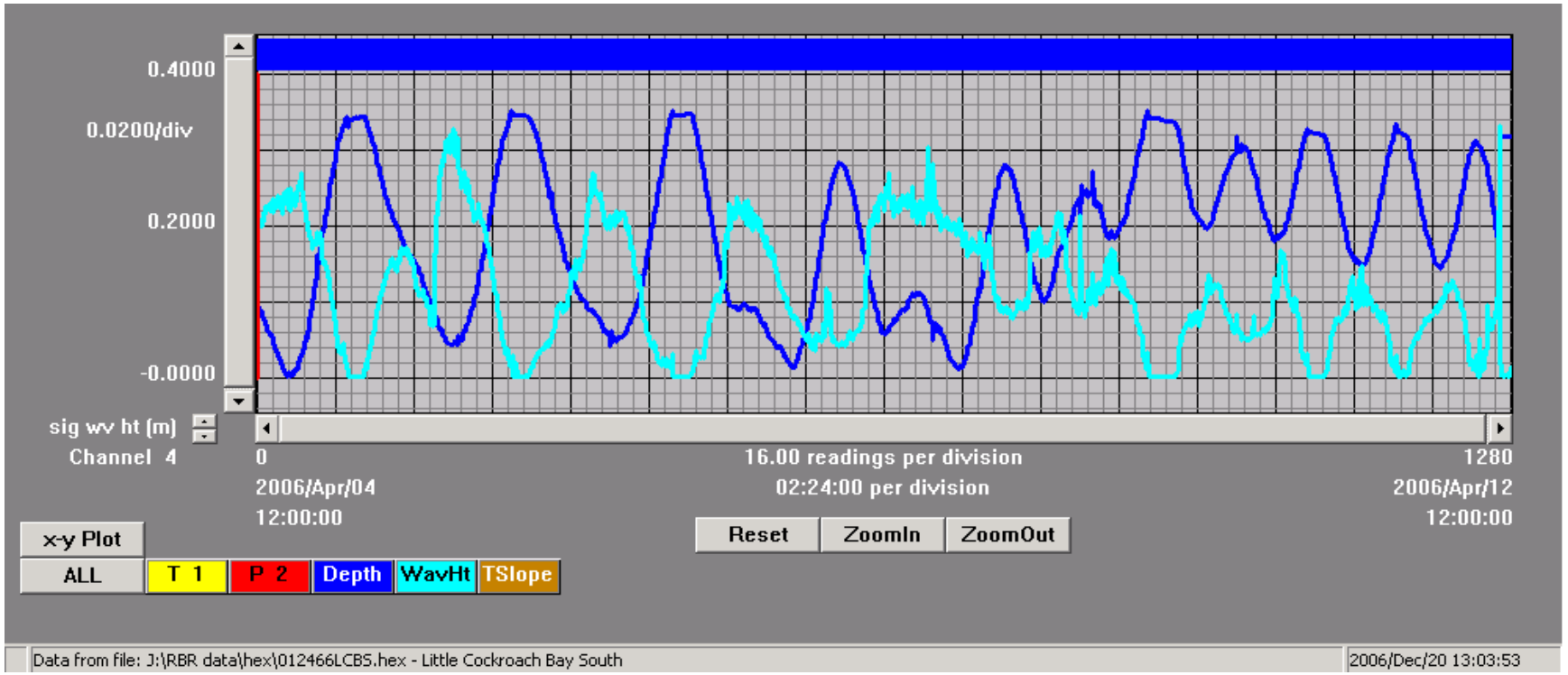

Figure 19: RBR data summary from Piney Point. These data represent wave heights (H_{max}) and depth on the bar or its analog. Data were collected from April 4 – April 12, 2006.

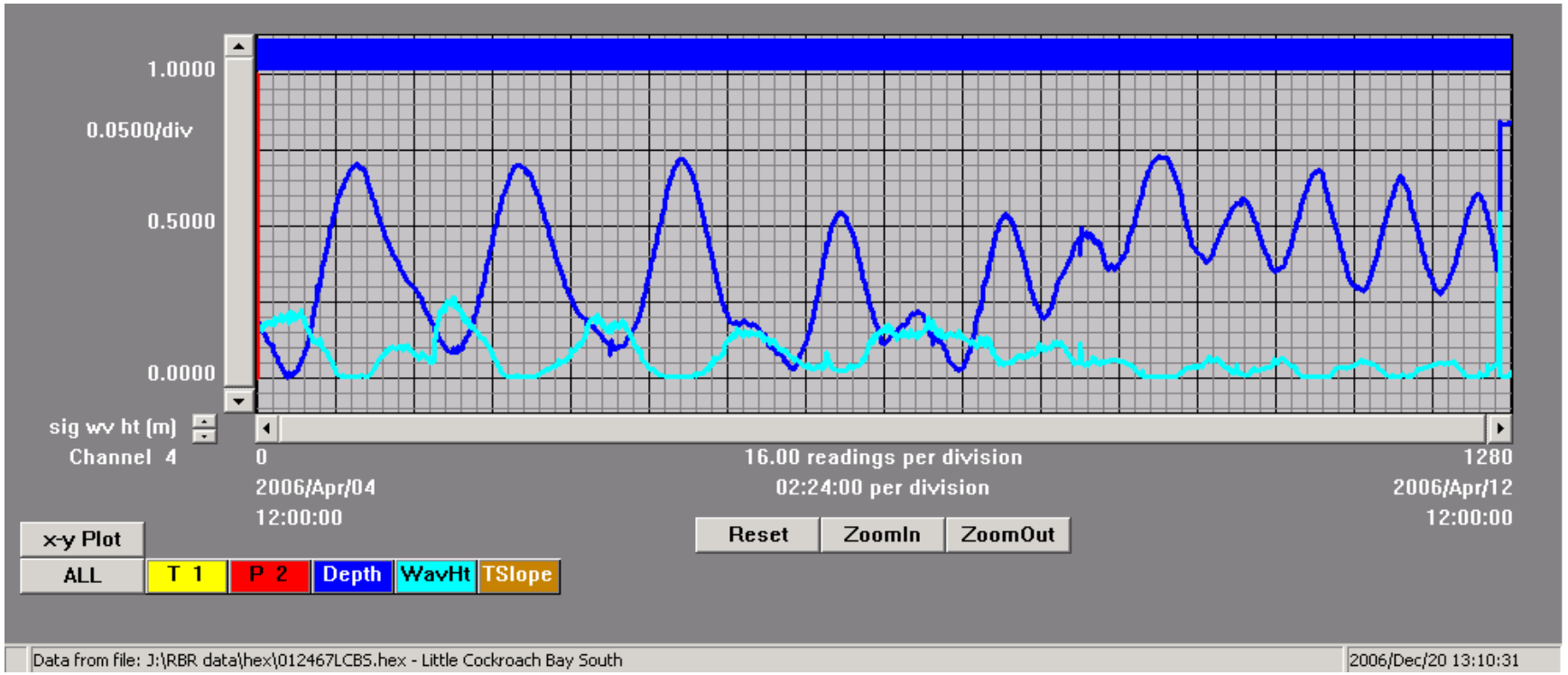

Figure 20: RBR data summary from Piney Point. These data represent wave heights (H_{max}) and depth behind the bar or its analog. Data were collected from April 4 – April 12, 2006.

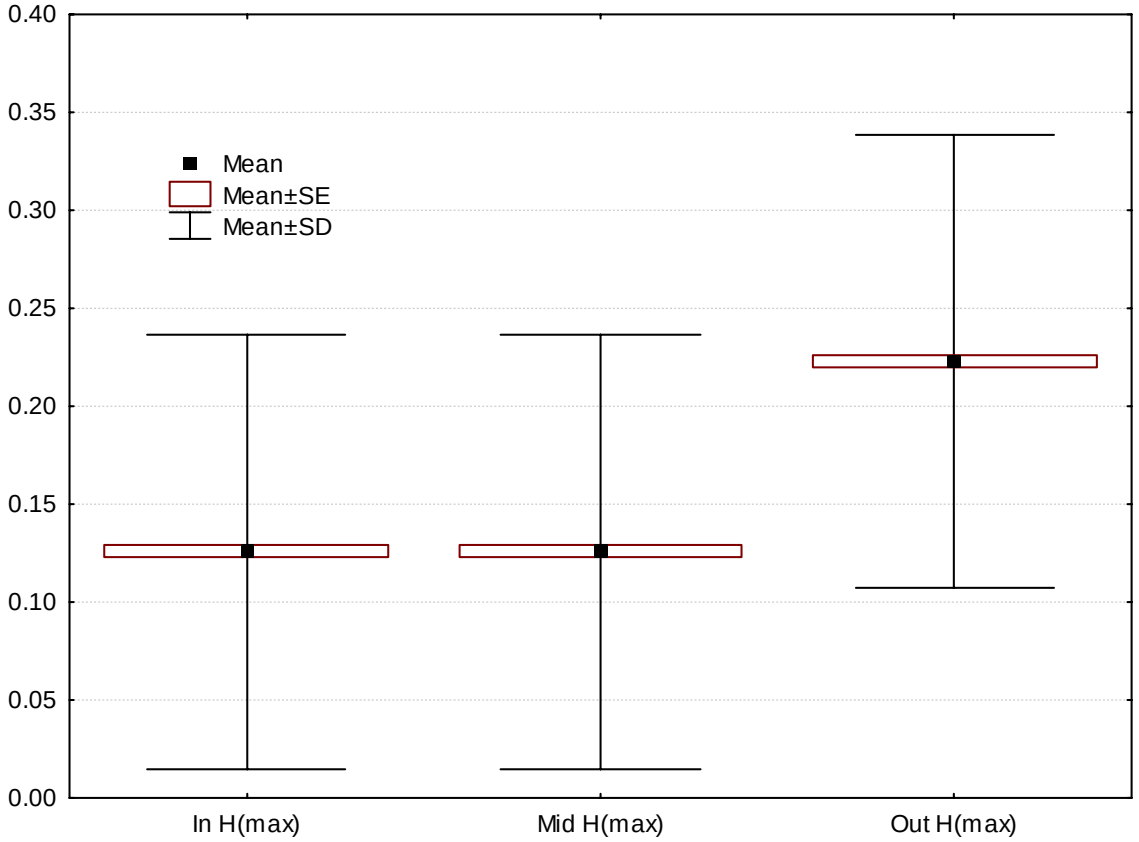

Figure 21: Box and Whisker plot depicting the relationship among instrument locations at the Piney Point site. Differences are significant at $p < 0.0001$.

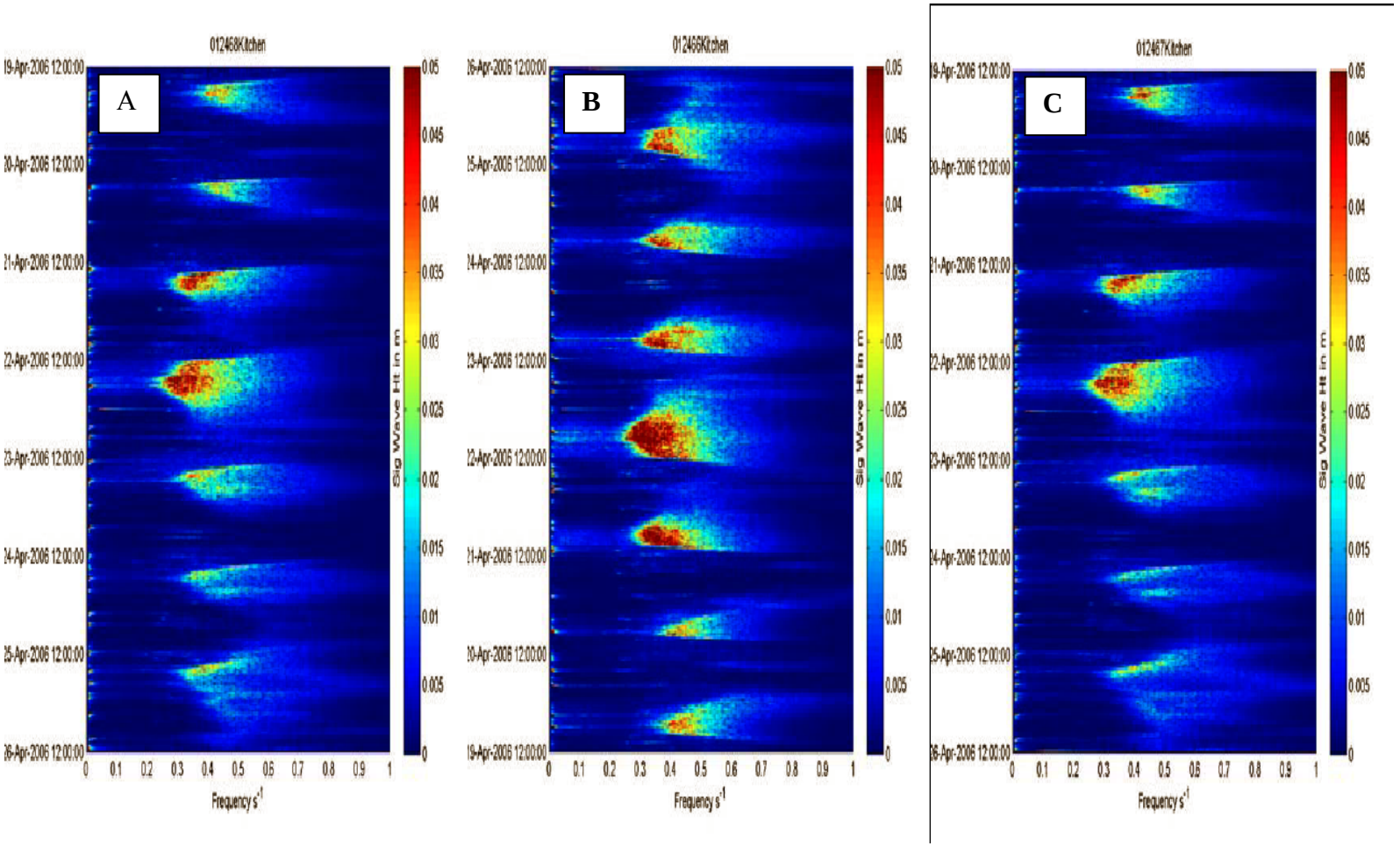

Figure 22: Results from fast Fourier transform of each wave burst for Kitchen offshore (a), Kitchen on-bar (b), and Kitchen inshore (c). Notice increased wave energy from 0.3 to 0.6 s^{-1} frequency band. This figure clearly shows that this energy modulates diurnally.

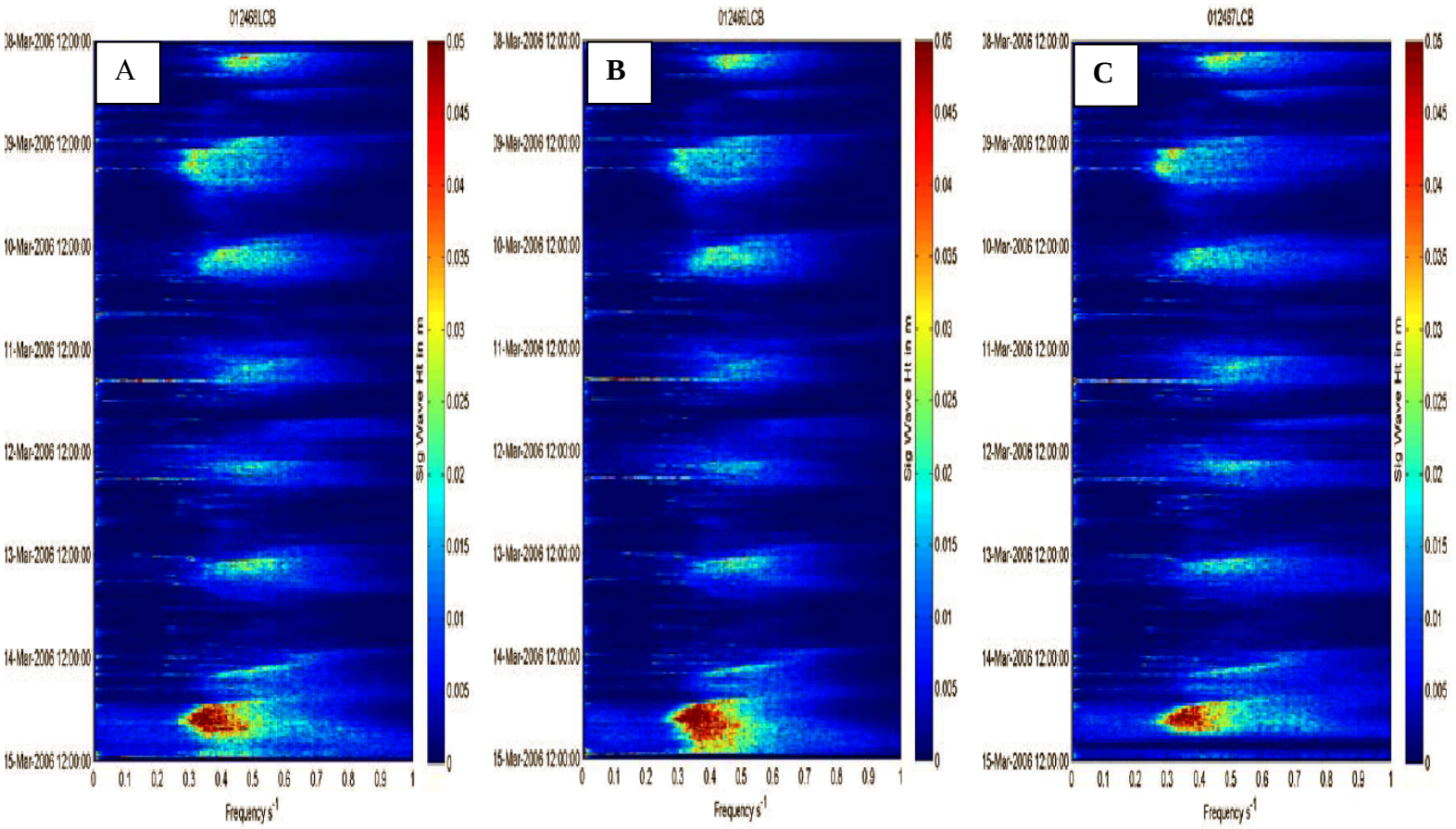

Figure 23: Results from fast Fourier transform of each wave burst for Lower Cockroach Bay offshore (a), Lower Cockroach Bay on-bar (b), and Lower Cockroach Bay inshore (c). Notice increased wave energy from 0.3 to 0.6 s^{-1} frequency band. This figure clearly shows that this energy modulates diurnally.

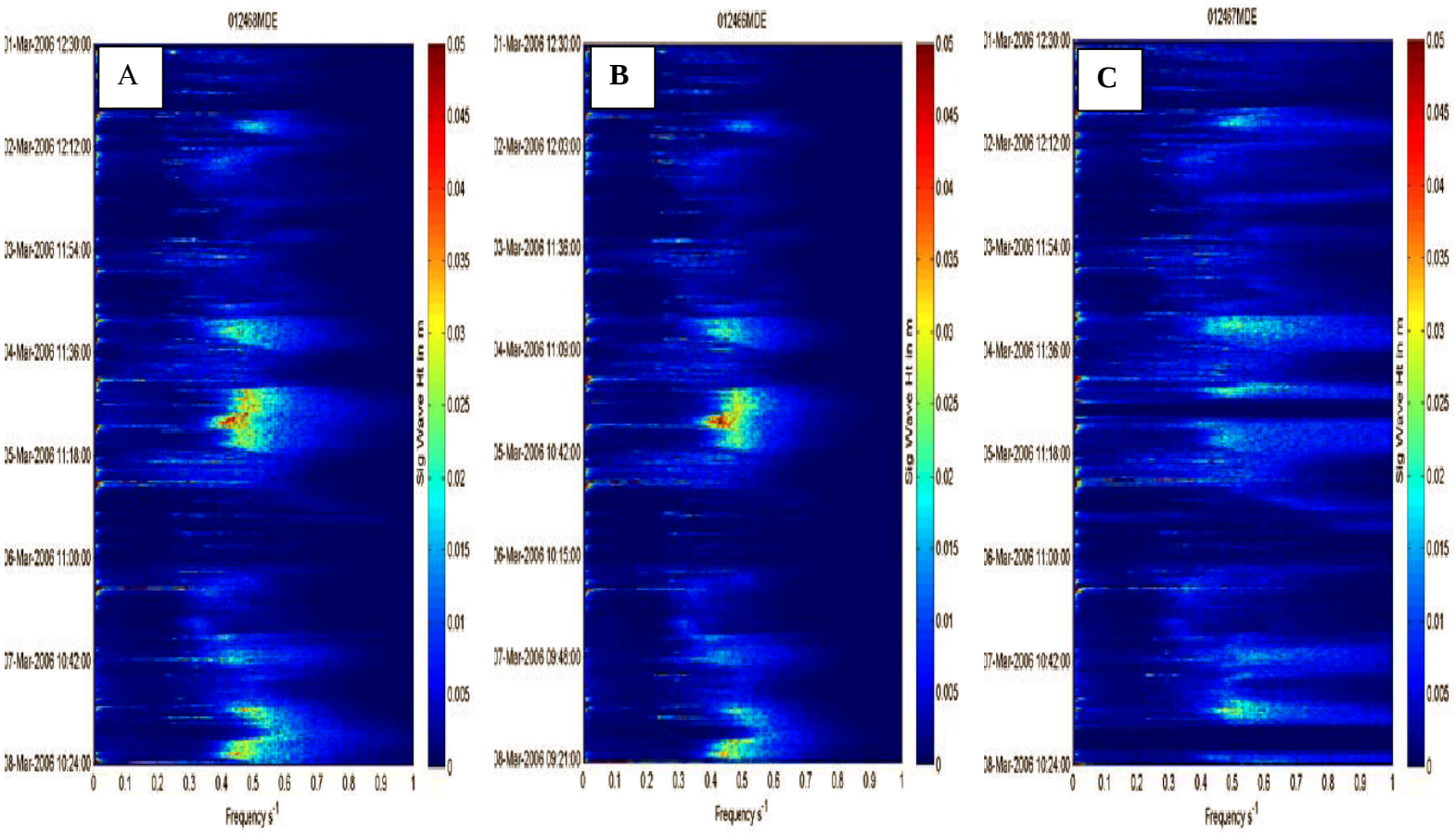

Figure 24: Results from fast Fourier transform of each wave burst for MacDill East offshore (a), MacDill East on-bar (b), and MacDill East inshore (c). Notice increased wave energy from 0.3 to 0.6 s^{-1} frequency band. This figure clearly shows that this energy modulates diurnally.

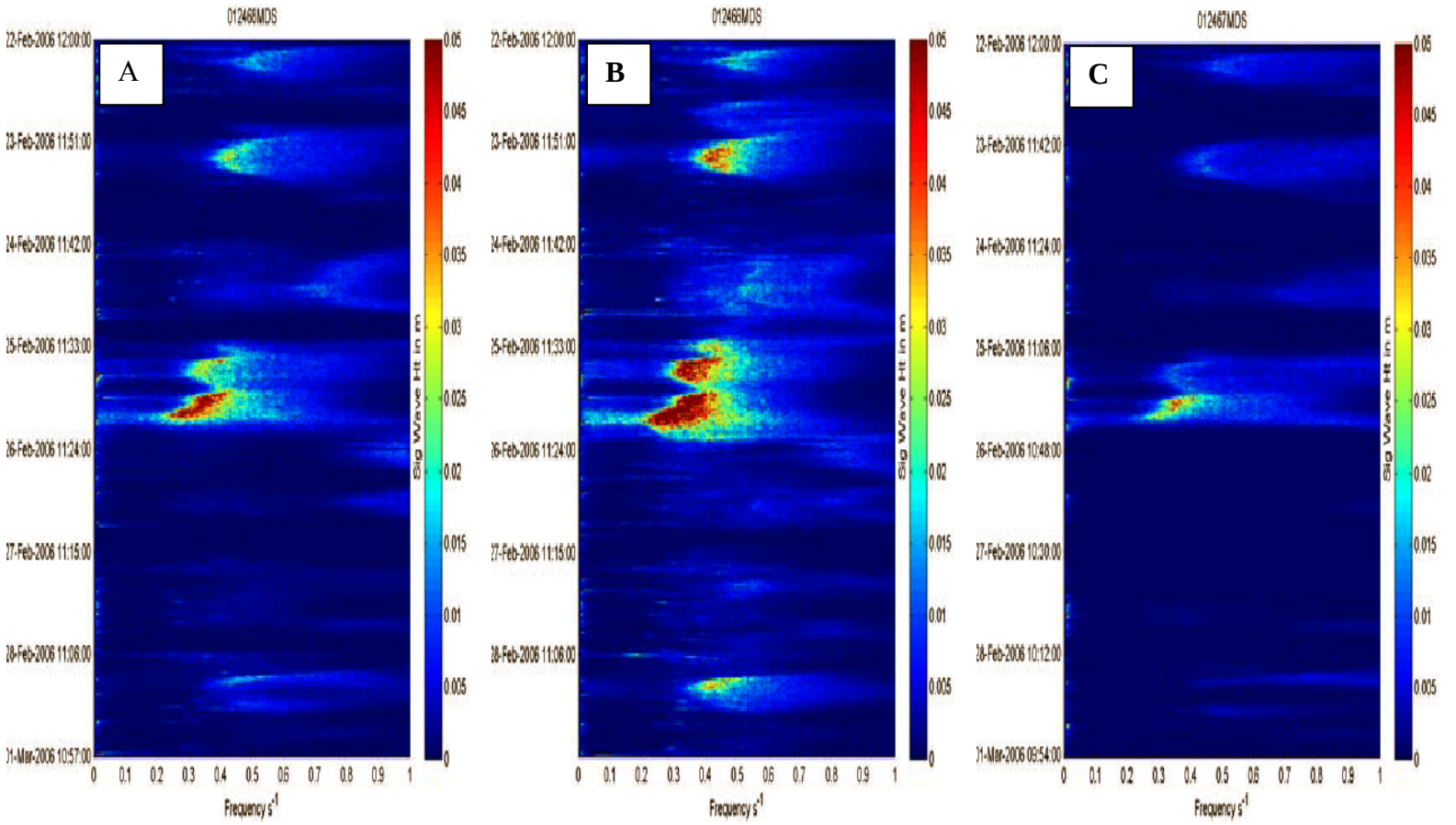

Figure 25: Results from fast Fourier transform of each wave burst for MacDill South offshore (a), MacDill South on-bar (b), and MacDill South inshore (c). Notice increased wave energy from 0.3 to 0.6 s^{-1} frequency band. This figure clearly shows that this energy modulates diurnally.

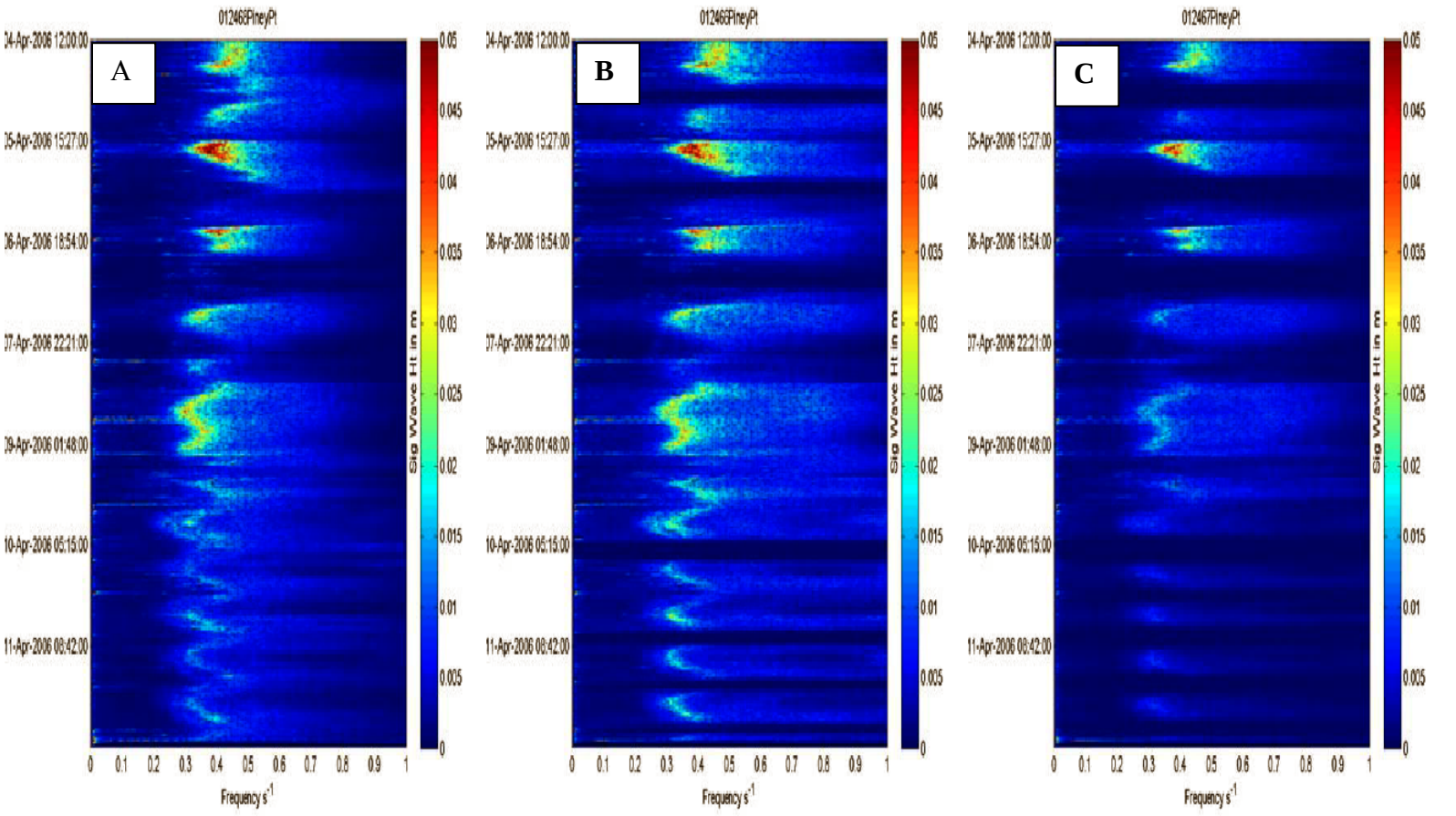

Figure 26: Results from fast Fourier transform of each wave burst for Piney Point offshore (a), Piney Point on-bar (b), and Piney Point inshore (c). Notice increased wave energy from 0.3 to 0.6 s^{-1} frequency band. This figure clearly shows that this energy modulates diurnally.

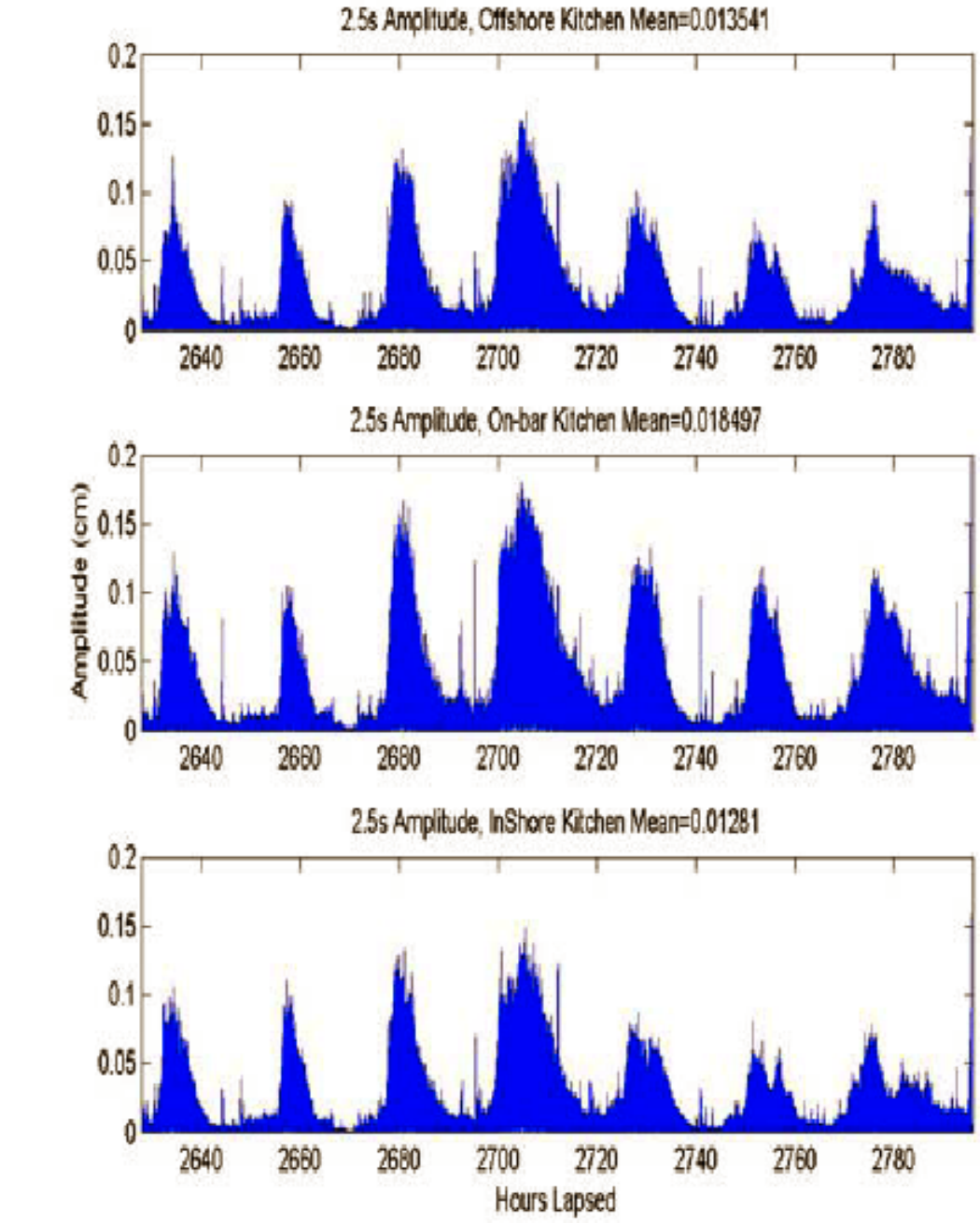

Figure 27: Demodulated series of 2.5 second variability at the Kitchen. Plots represent offshore (top), on-bar (middle), and inshore (bottom) observations. The overall mean amplitude is included in the title.

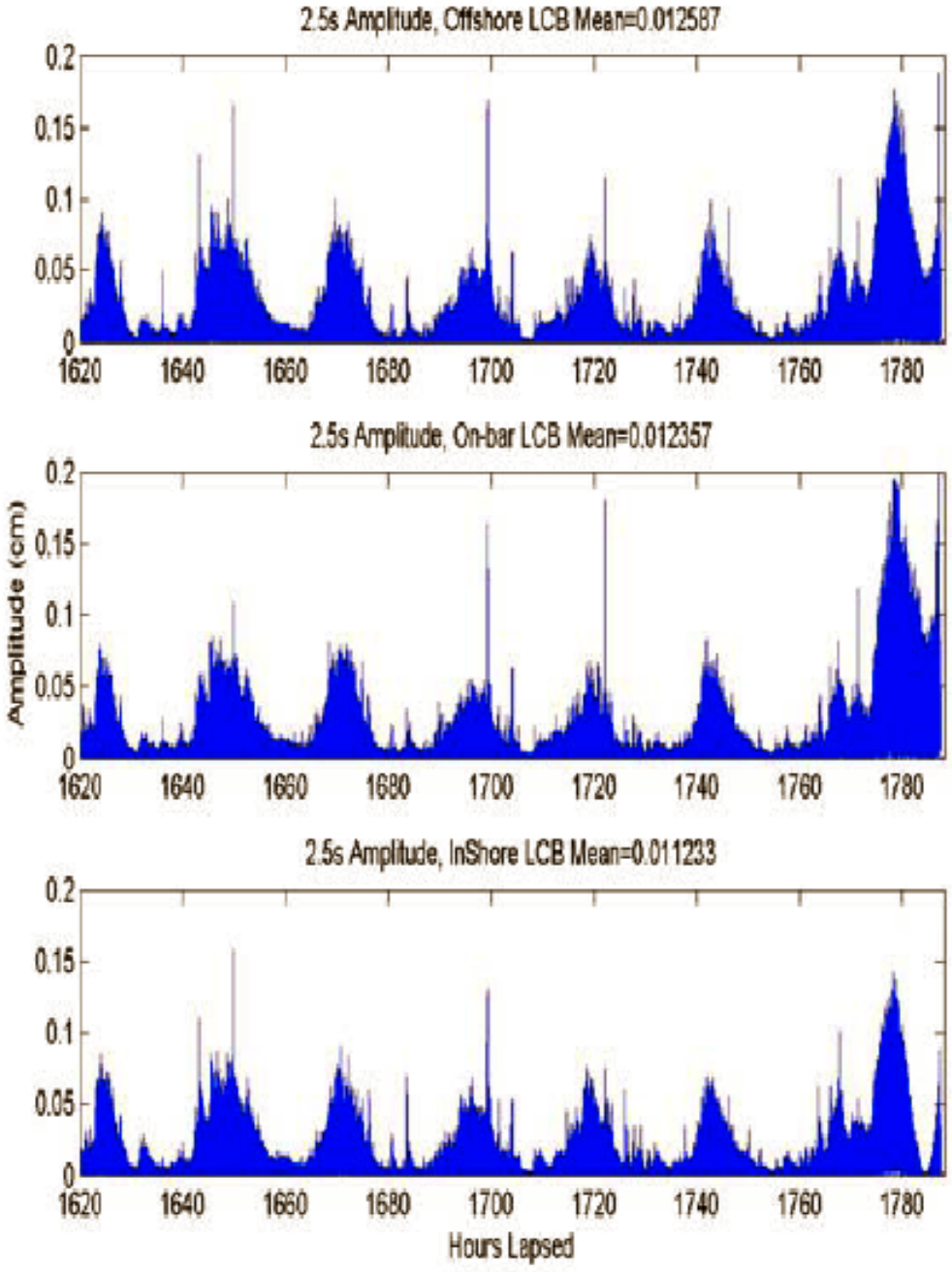

Figure 28: Demodulated series of 2.5 second variability at Little Cockroach Bay. Plots represent offshore (top), on-bar (middle), and inshore (bottom) observations. The overall mean amplitude is included in the title.

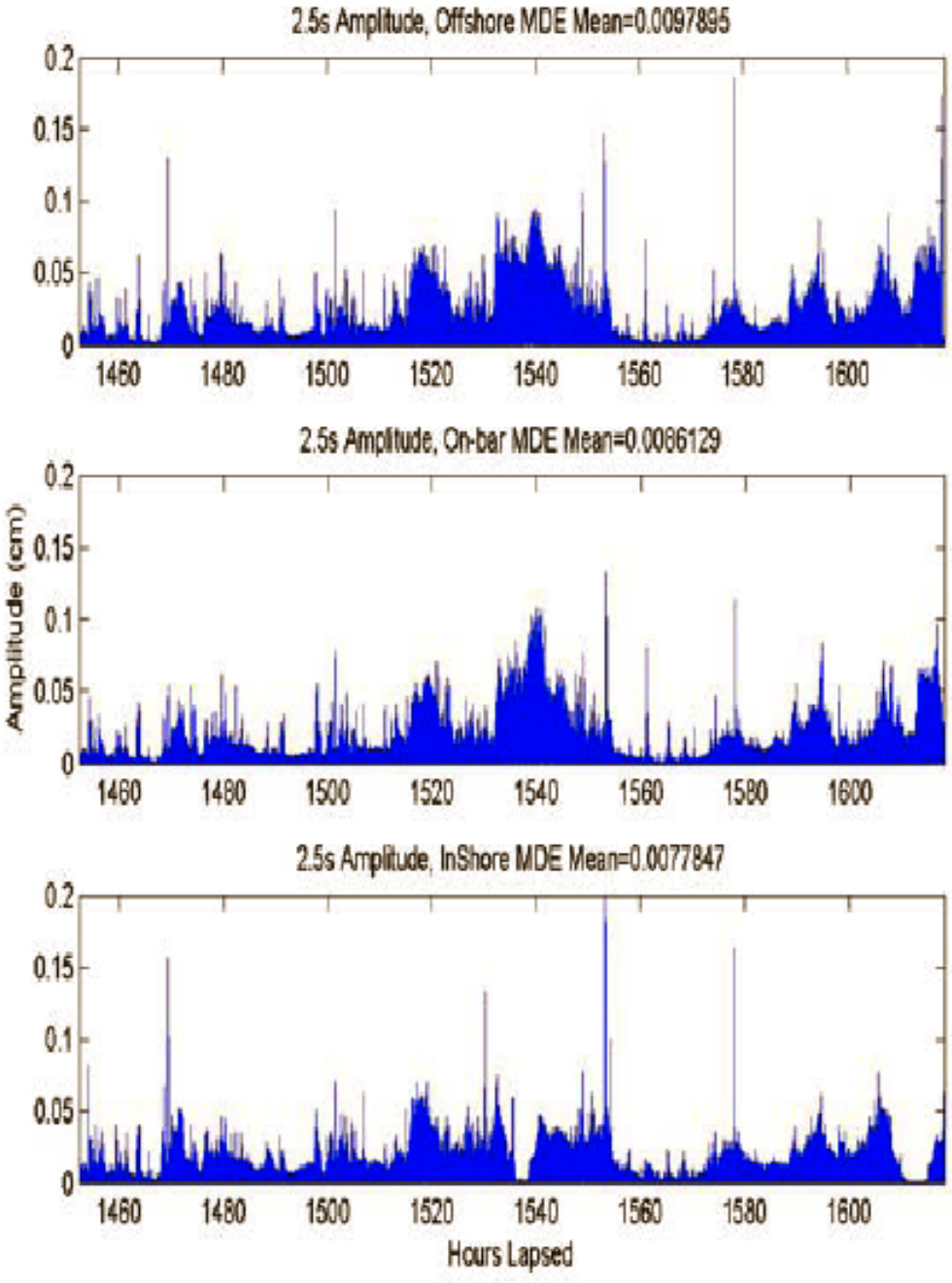

Figure 29: Demodulated series of 2.5 second variability at MacDill East. Plots represent offshore (top), on-bar (middle), and inshore (bottom) observations. The overall mean amplitude is included in the title.

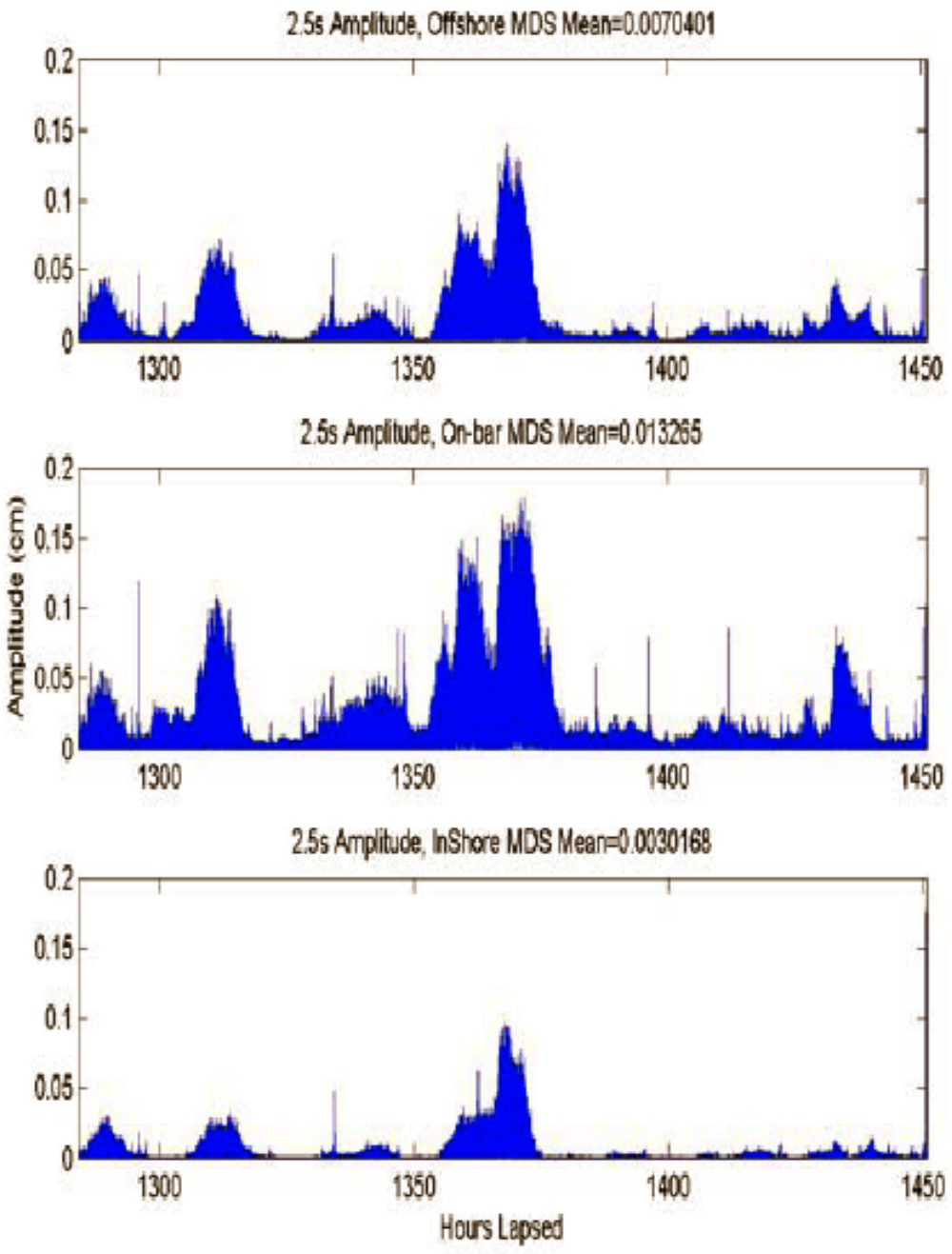

Figure 30: Demodulated series of 2.5 second variability at MacDill South. Plots represent offshore (top), on-bar (middle), and inshore (bottom) observations. The overall mean amplitude is included in the title.

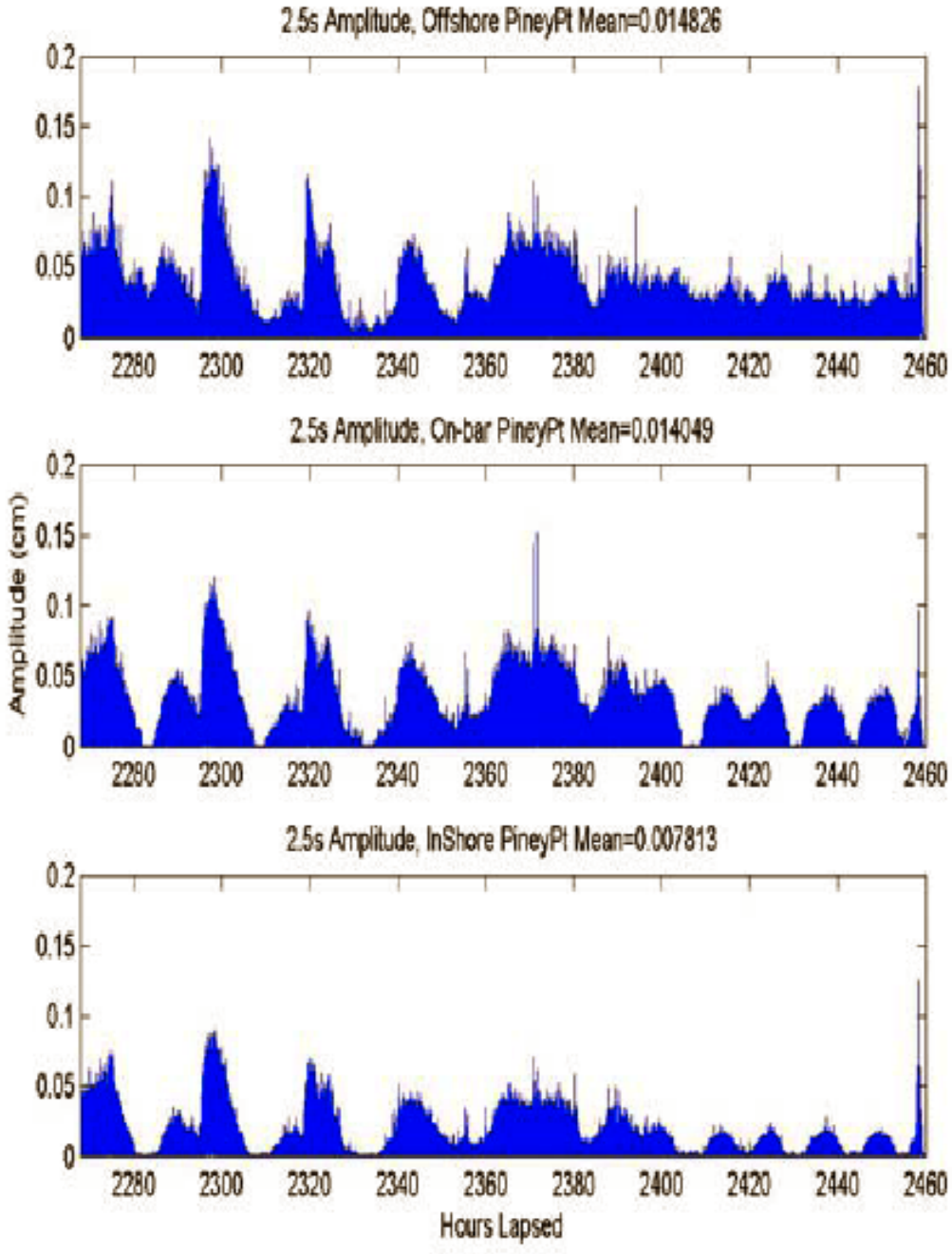

Figure 31: Demodulated series of 2.5 second variability at Piney Point. Plots represent offshore (top), on-bar (middle), and inshore (bottom) observations. The overall mean amplitude is included in the title.

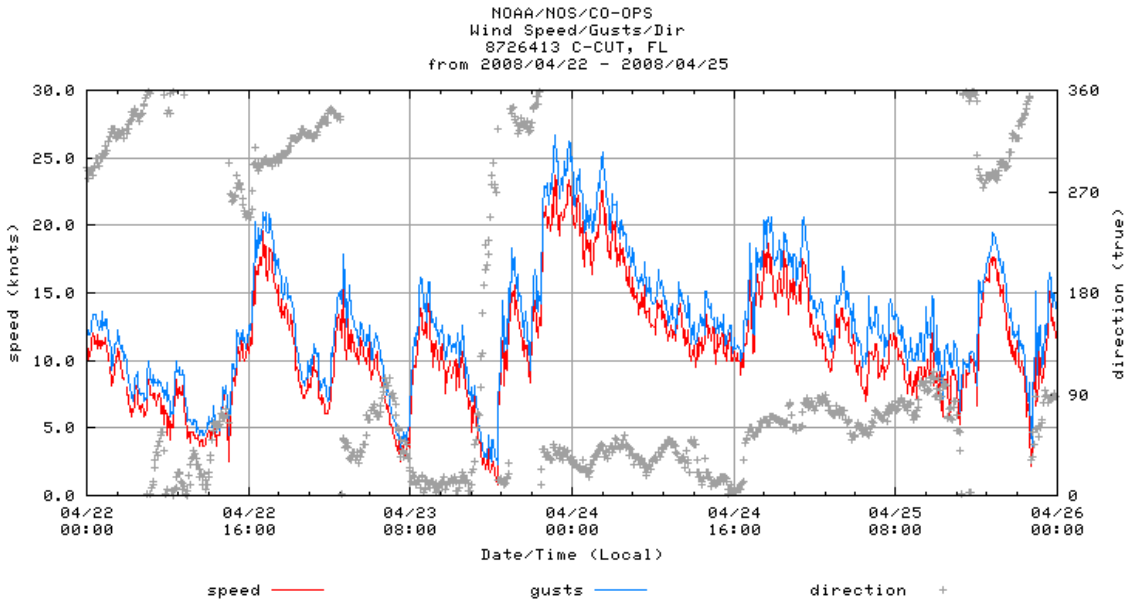

Figure 32: Wind data during the Coffee Pot Bayou deployment from the NOS TB-PORTS C-CUT site in mid-Tampa Bay. Winds exceeded 25 knots from the Northeast on 4/24/08.

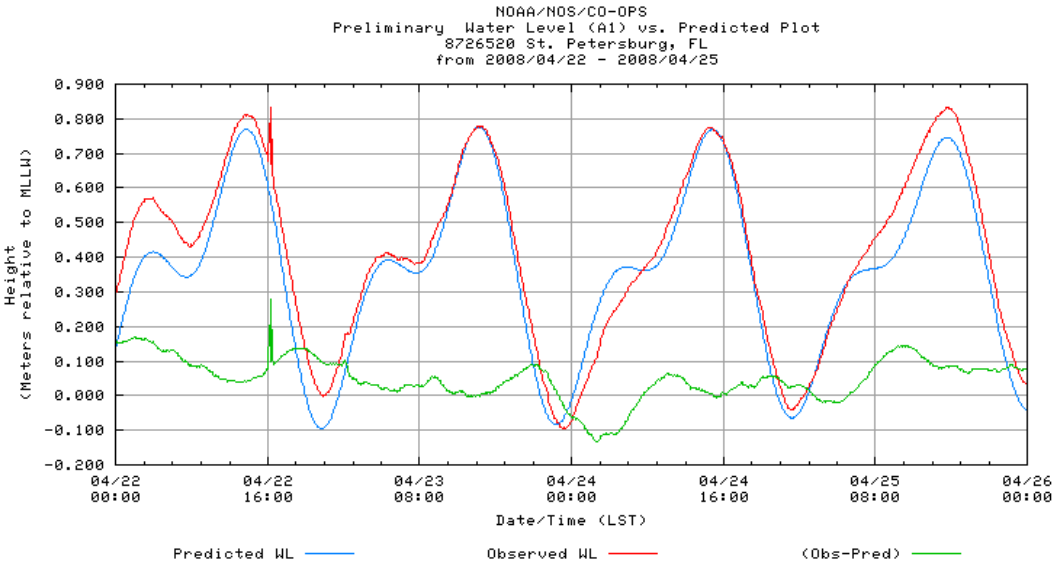

Figure 33: Water level data during the Coffee Pot Bayou deployment from the NOS TB-PORTS St. Petersburg site indicating spring tidal conditions between April 23-24.

Figure 34: Locations of Coffeepot Bayou deployment. Red circles indicate inshore and offshore sites.

Figure 35: Locations of MacDill deployment. Red circles indicate inshore and offshore sites. These sites are just inshore and offshore of a proposed site for the installation of submerged bars.

Fig. 36a:

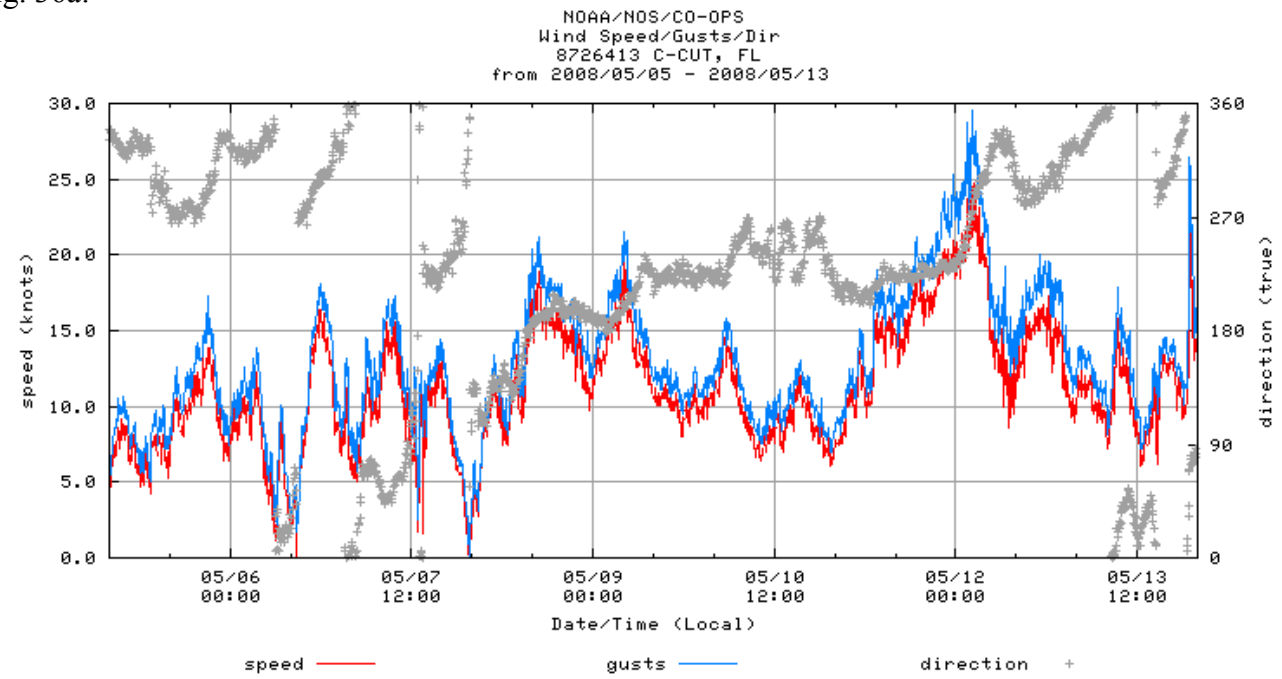

Fig 36b:

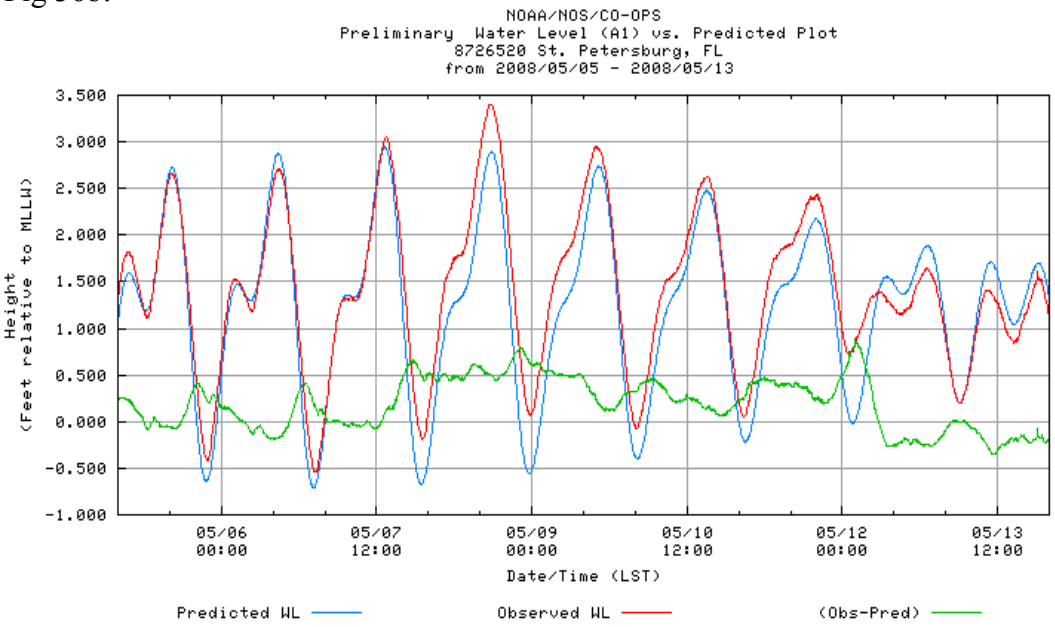

Figure 36: (a) Wind speed and direction from the mid-bay NOS TB-POTYS site. Winds were from the SW at 10 to 20 knots from 5/8 to 5/12, reaching 25 to 30 knots on 5/12. (b) Water level during the MacDill deployment from the NOS TB-PORTS St. Petersburg water level site. Spring tide occurred on 5/7 to 5/9, with a range of 3.5 ft. Water level was 0.5 to 0.8 ft. above predicted due to strong southerly winds over much of this period.

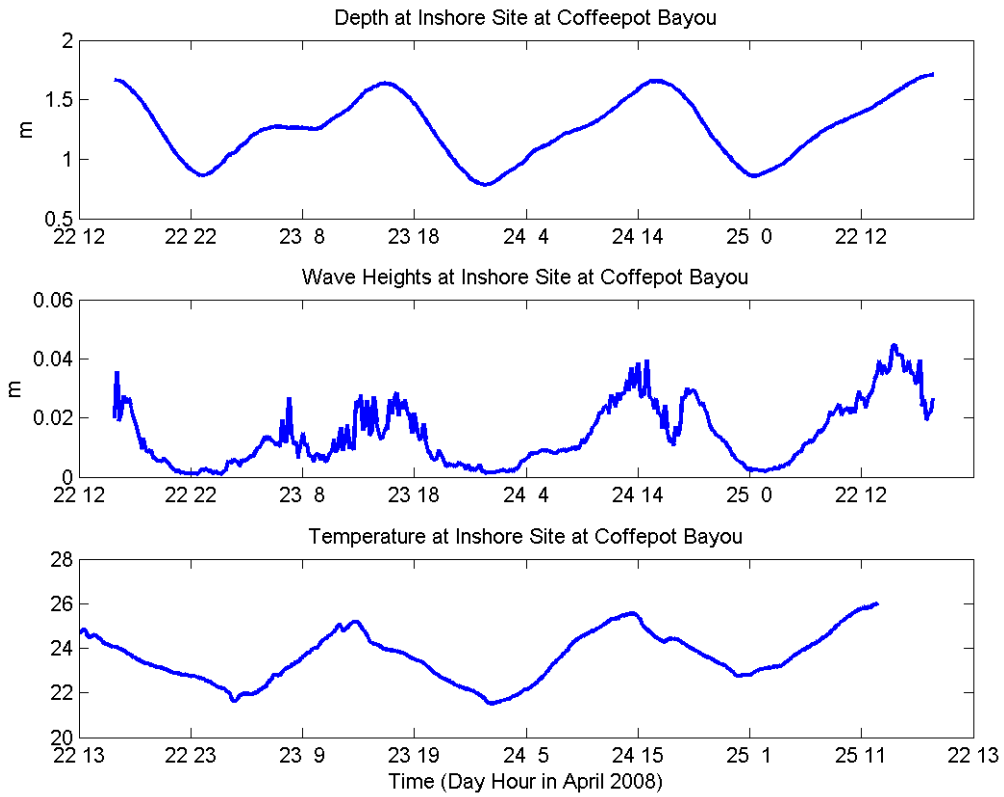

Figure 37: Depth, Wave Heights ($H_{1/3}$), and Temperature from Coffeepot Inshore Site

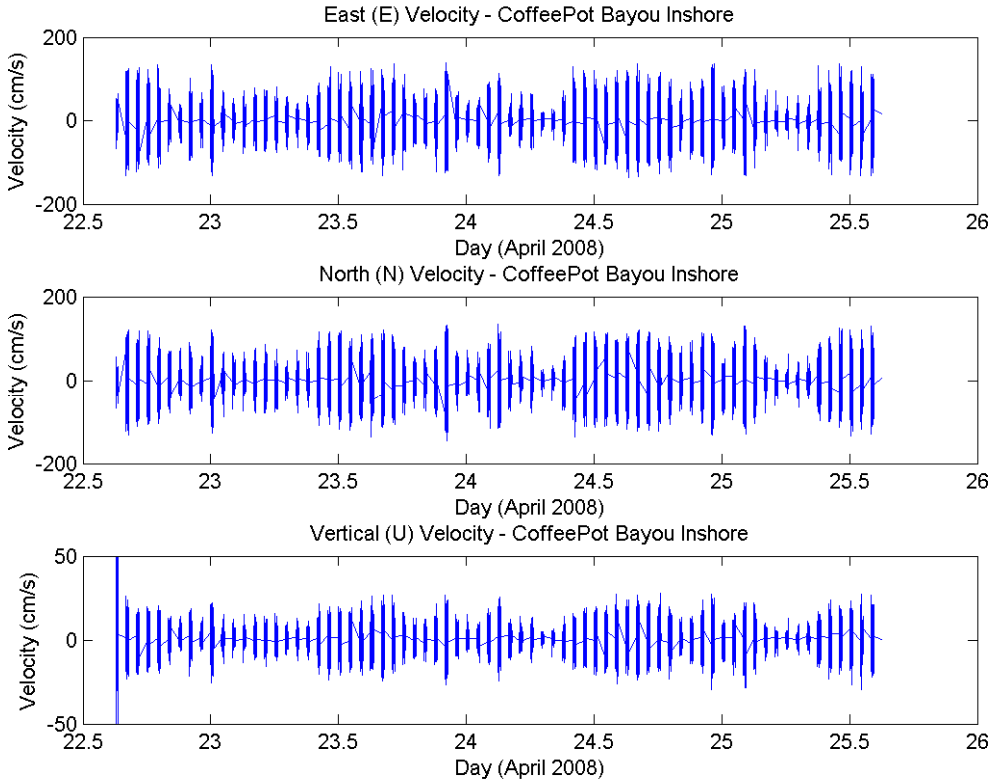

Figure 38: Sontek ADP data from Coffeepot Bayou Inshore Site

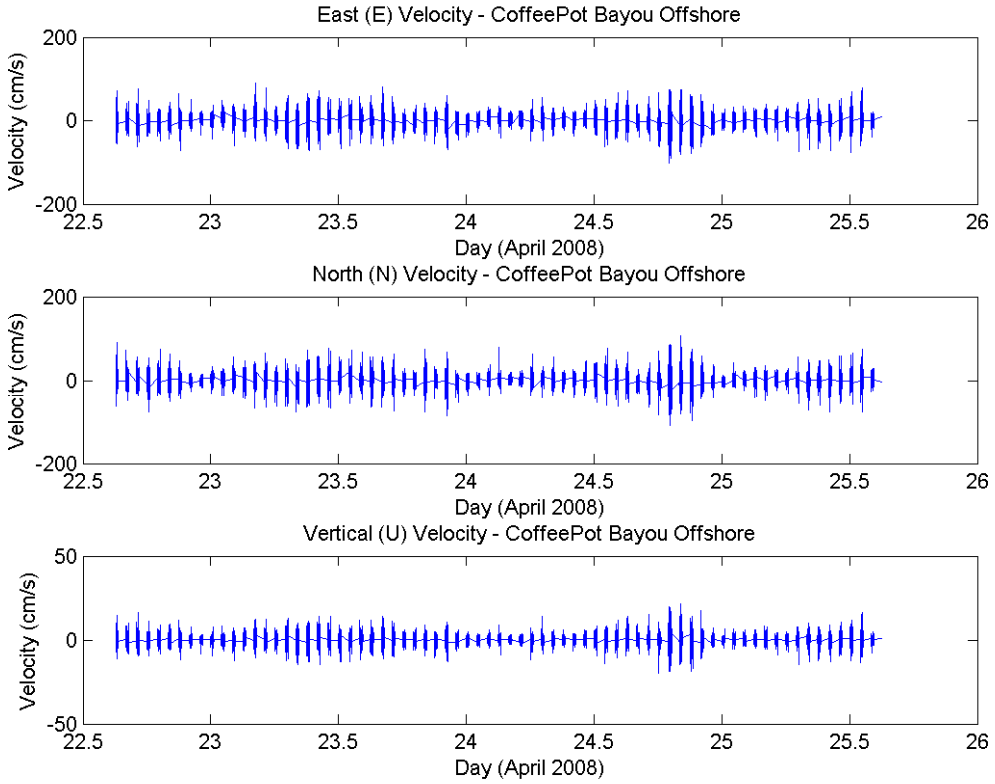

Figure 39: Sontek ADP data from Coffeepot Bayou Offshore Site

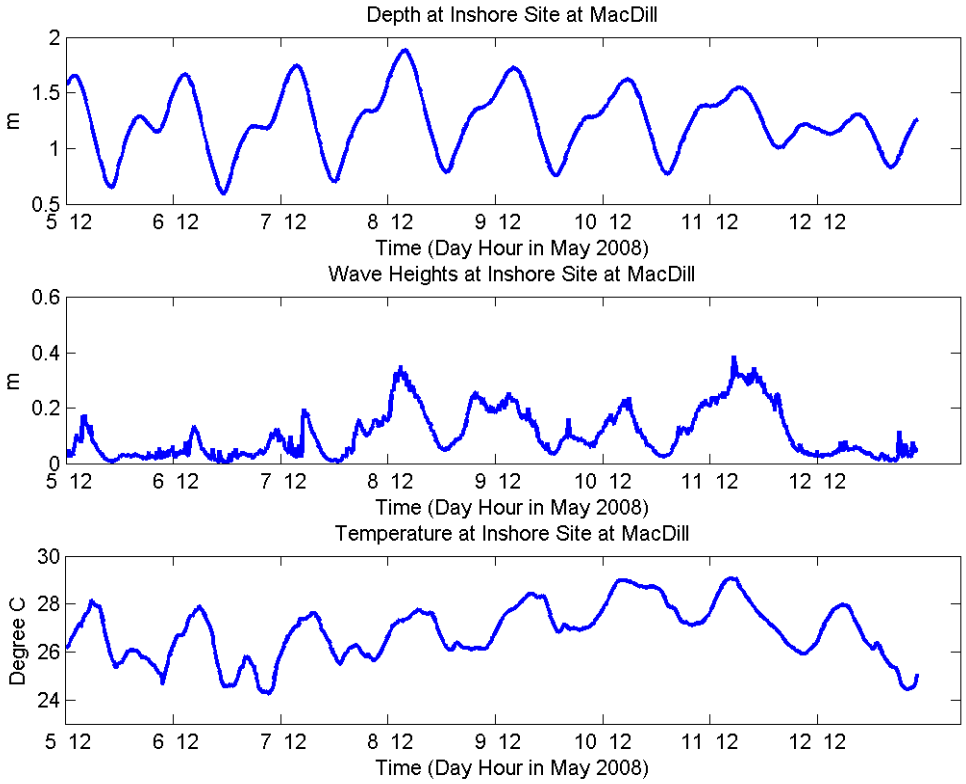

Figure 40: Depth, Wave Heights ($H_{1/3}$), and Temperature from MacDill Inshore Site

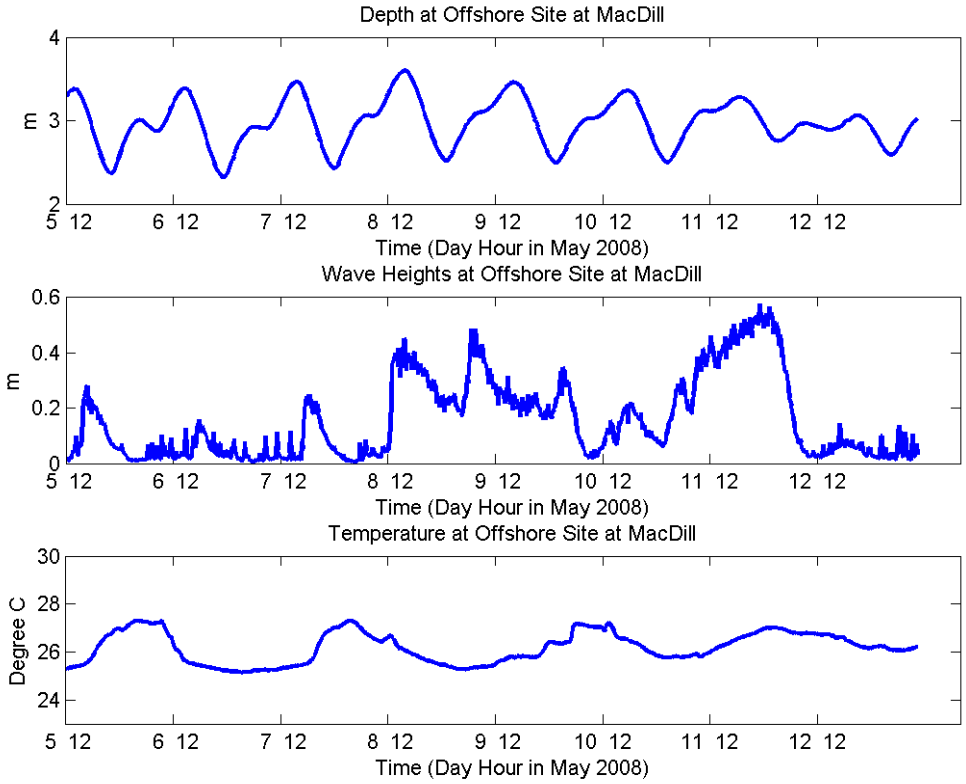

Figure 41: Depth, Wave Heights ($H_{1/3}$), and Temperature from MacDill Offshore Site

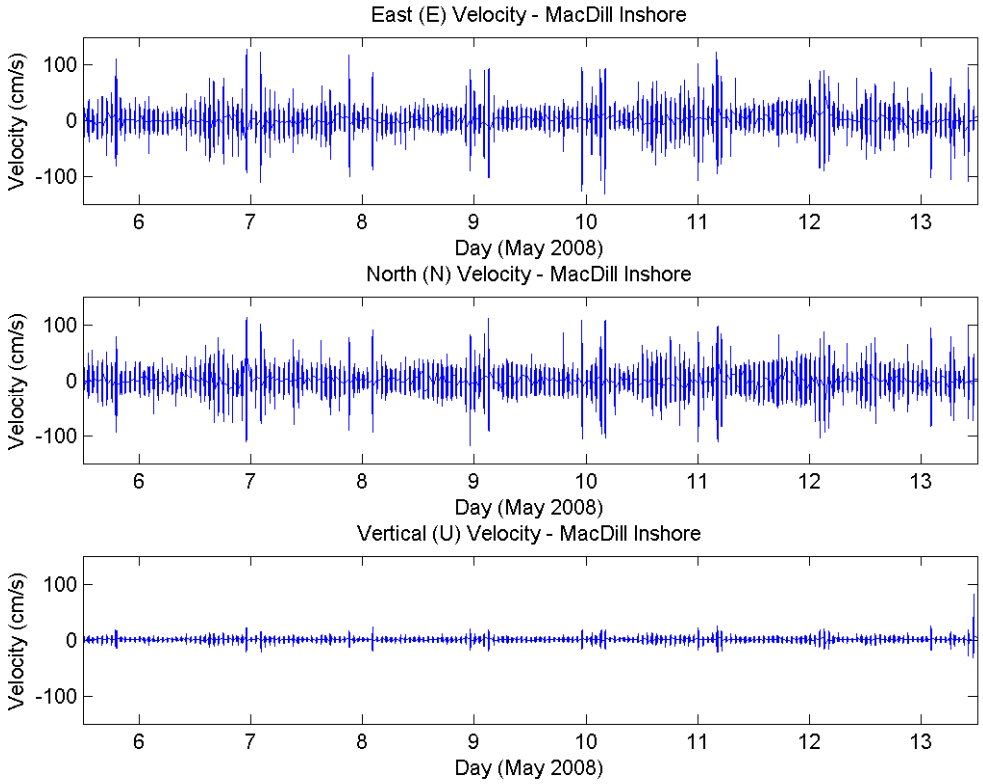

Figure 42: Sontek ADP data from MacDill Inshore Site

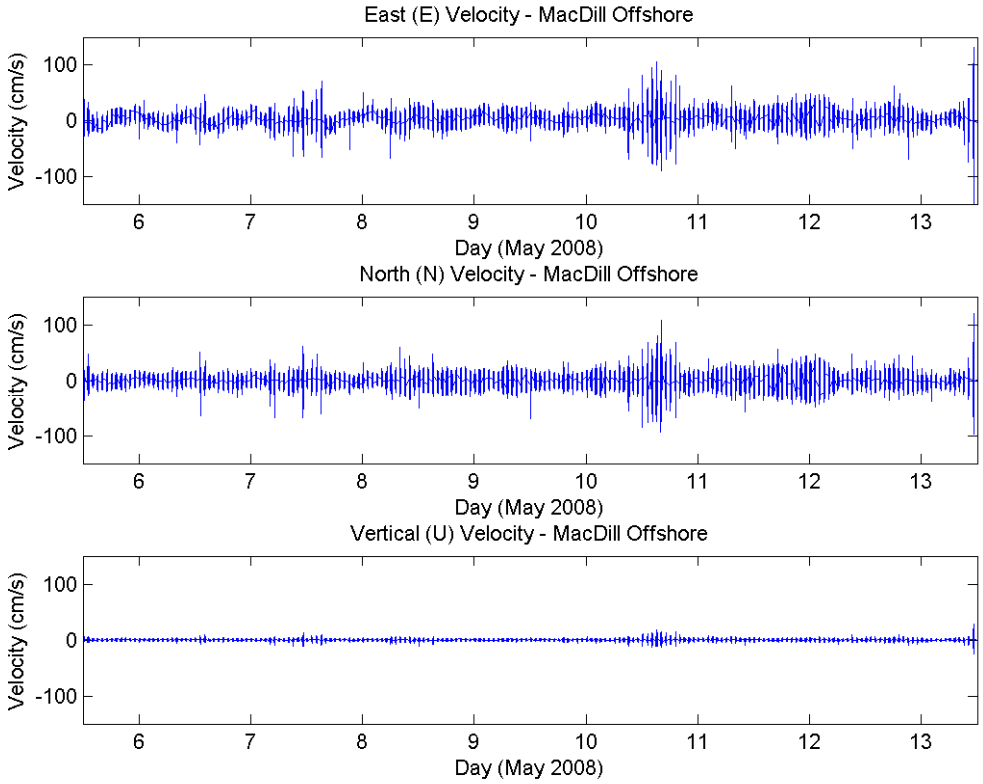

Figure 43: Sontek ADP data from MacDill Offshore Site

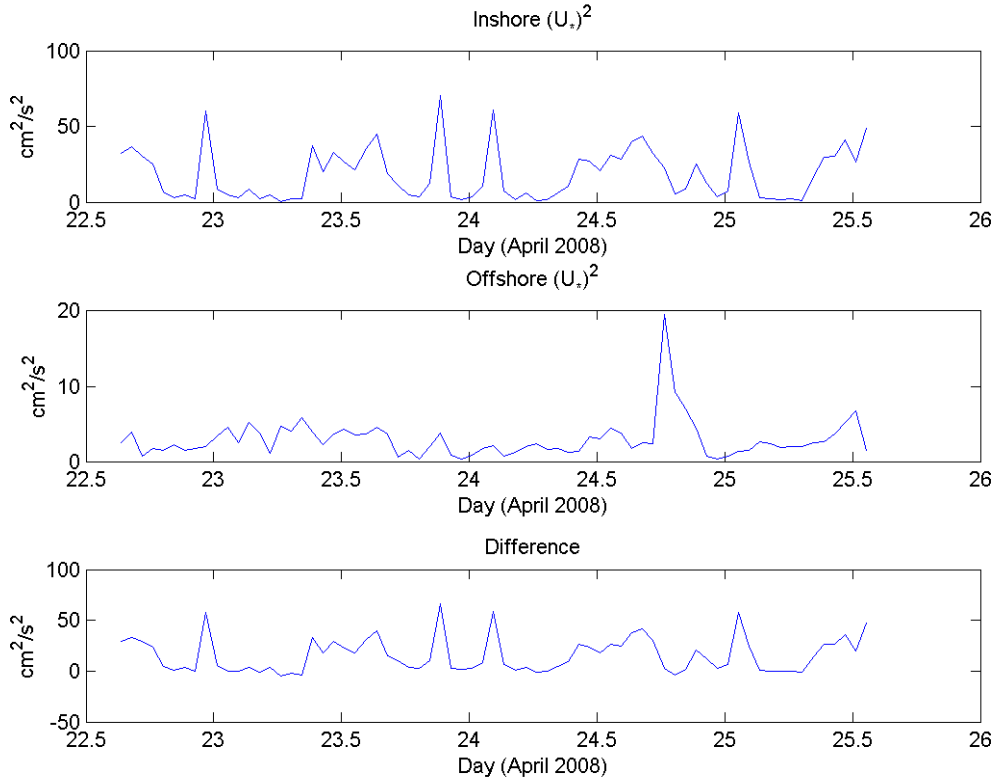

Figure 44: Computed friction velocities at Coffeepot Bayou.

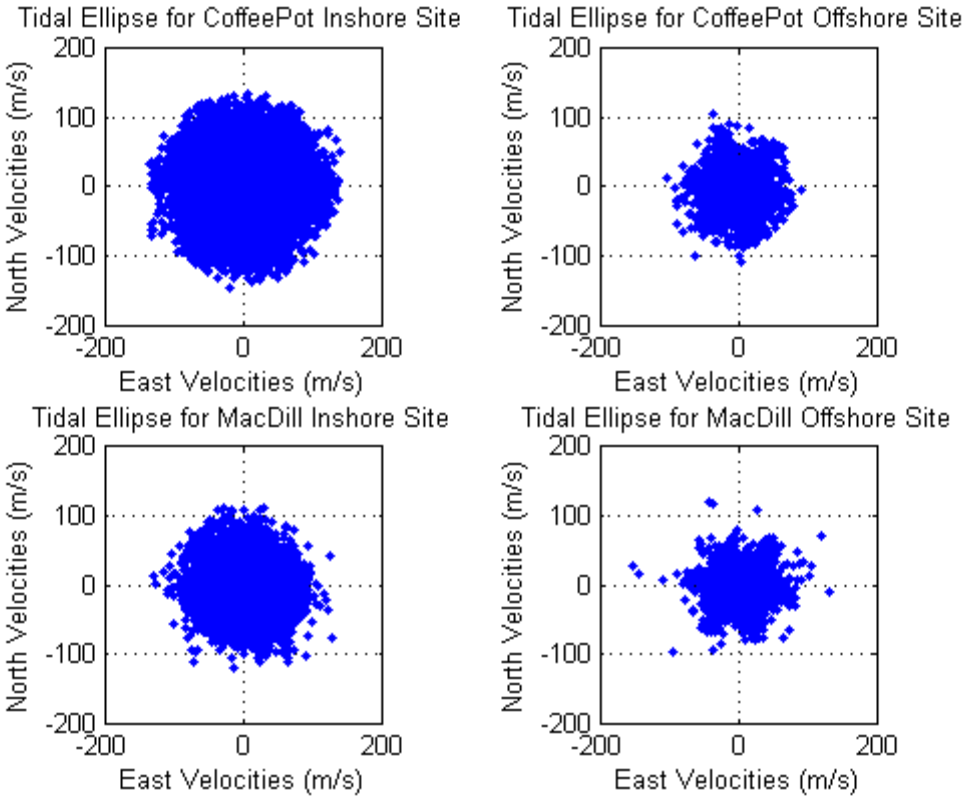

Figure 45: Tidal ellipses for all sites. Velocities are centered around (0,0) indicating to preferred flow direction. This view shows the larger velocities inshore for both locations as indicated in the text.

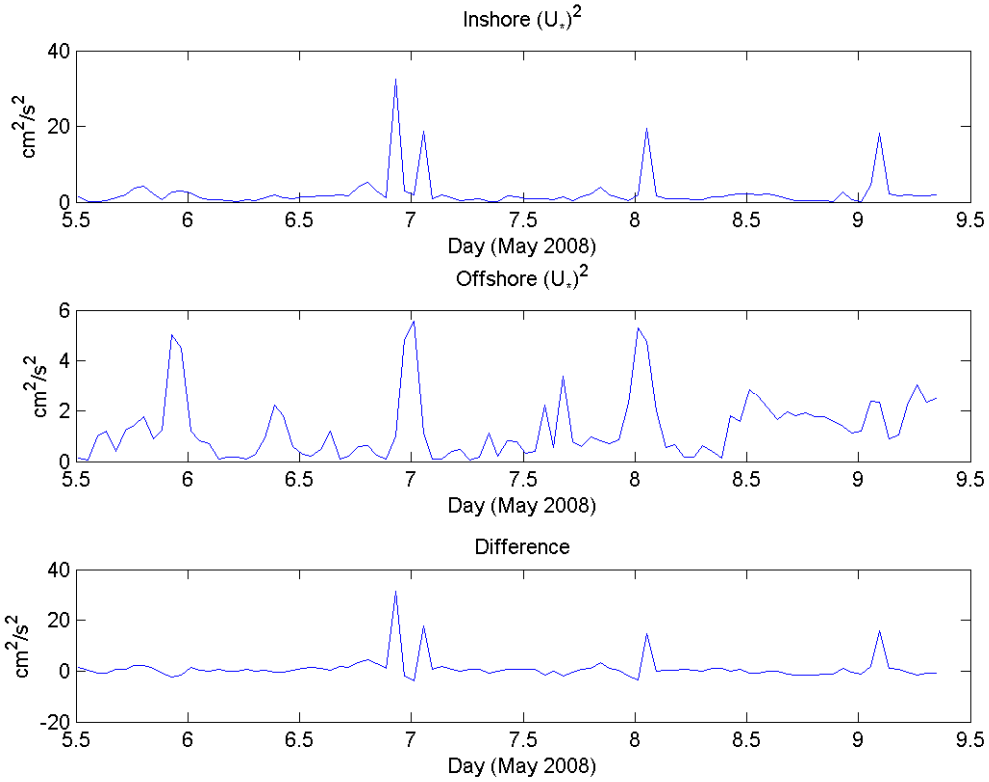

Figure 46: Computed Friction Velocity at MacDill Sites

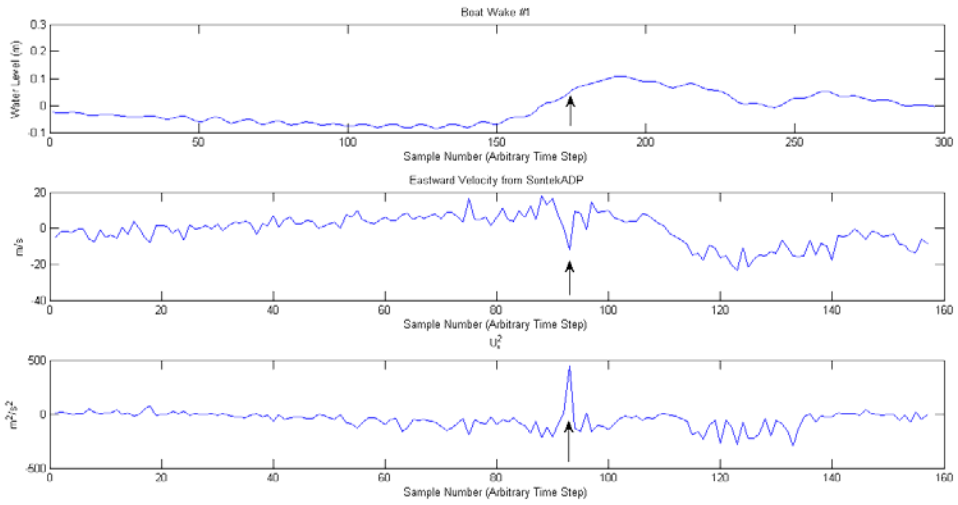

Figure 47: Example 1 of a boat wake at the MacDill Offshore site

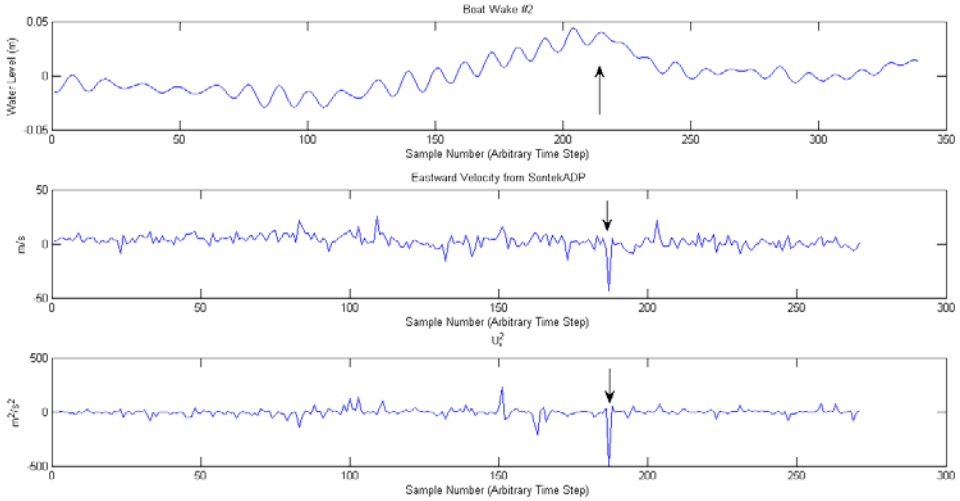

Figure 48: Example 2 of a boat wake at the MacDill Offshore site

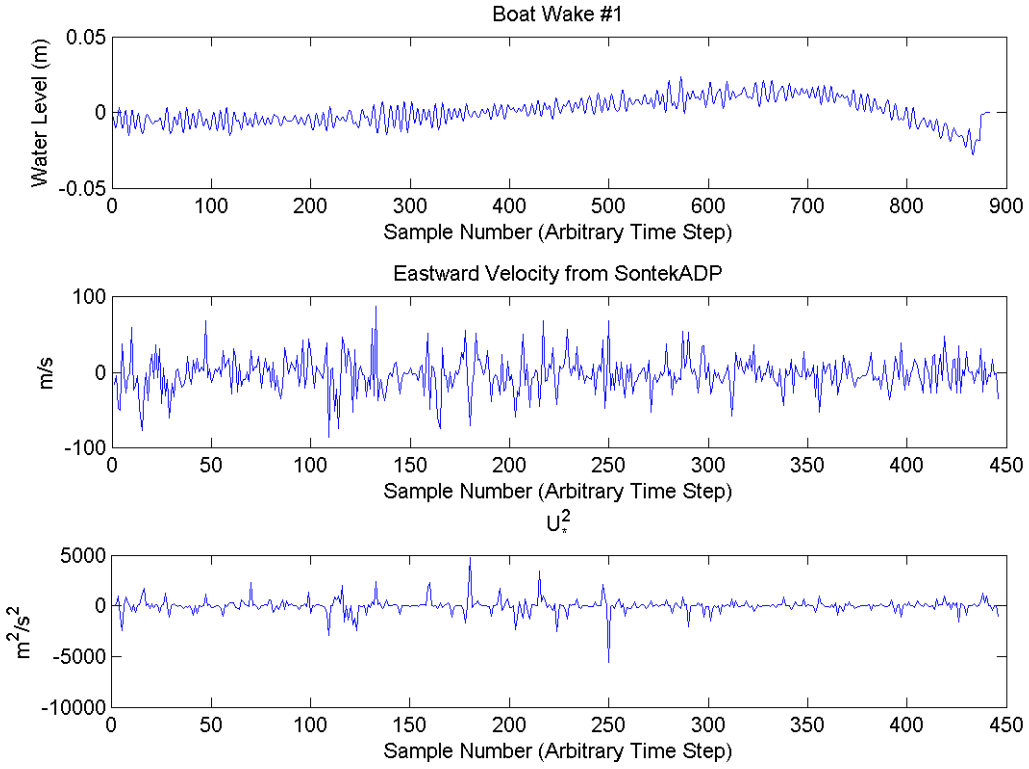

Figure 49: Example 1 of a boat wake at the MacDill Inshore site

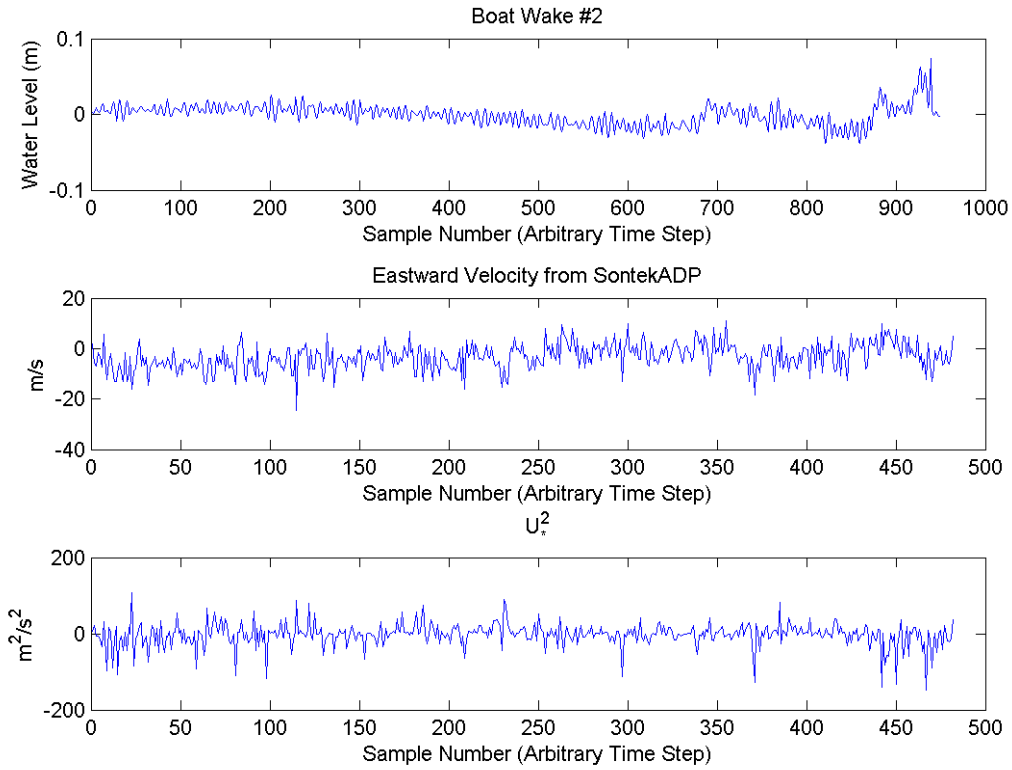

Figure 50: Example 2 of a boat wake at the MacDill Inshore site

Fig. 51a:

Fig. 51b:

Figure 51: (a) PC ADP at the beginning of the MacDill deployment at the outer site (approximately 8 to 10 ft depth at MLLW). (b) At the end of the deployment – considerable sediment erosion and nascent barnacle accumulation are evident.